MARMARA UNIVERSITY

FACULTY OF ENGINEERING

NUMERICAL ANALYSIS OF PREMIXED HYDROGENATED METHANE COMBUSTION ON A LABORATORY SCALE CHAMBER

Ömer Faruk ÇOLAK, Gürkan SAYILKAN

GRADUATION PROJECT REPORT

Department of Mechanical Engineering

Supervisor

Doç.Dr. Barış YILMAZ

ISTANBUL, 2022

Table of Contents

List of Figures

List of Tables

ABSTRACT

Global warming is getting worse day to day. The reason for the global warming is greenhouse gases. Greenhouse gas consists of CO_2 , CO, NO_x , SO_x . The main producer of greenhouse gasses is combustion. The high temperature of the combustion product produces NO_x. Thermal NO_x occurs when nitrogen and oxygen in the combustion air combine at the high temperatures in a flame. Thermal NO_x makes up most of the NO_x formed during the combustion of gases and light oils. The rate of NO_x formation generally raises especially above 1500°C flame temperature. Besides, the combustion of fossil fuels produces NO_x , SO_x .Methane is preferred instead of fossil fuel in the burner. The emission of NO_x , and SO_x in methane combustion is lower than a fossil fuel because methane has a flame temperature lower. The emission rate of methane combustion will not meet future emission values. According to Paris Agreement, decarbonization has been starting to be important in the next years. This reason causes starting to make research on decarbonization and reducing emissions. In this condition hydrogen is an option to decarbonize fuels and reduce emissions. Hydrogen combustions have lower flame temperatures. In lower flame temperatures NO_x emissions are going down. For that reason, it causes improved emission levels. Hydrogen fuels do have no carbon atoms. Thus, there is no carbon emission in hydrogen combustion. Due to hydrogen having a higher laminar flame speed for that reason hydrogen cannot be burned to own itself. Hydrogen can be mixed with methane in different equivalence ratios. The aim of this study is that simulate methane and hydrogen-methane flame in different equivalence ratios and investigate flame characteristics and properties.

In this study, premixed hydrogen doped methane/air flames were numerically investigated under lean mixture conditions. For this purpose, the geometry of the experimental setup was modeled in two dimensions, based on the data measured in the high-pressure combustion chamber experimental setup installed in the Institute of Orleans - ICARE (France). Modelling studies were carried out in various steps. In the first stage, the cold flow area in the combustion chamber was calculated numerically. In this modelling study, as in the experimental study, the air was chosen as the fluid. At the same time, the version of the standard k-ε turbulence model that showed the best agreement with the experimental data was determined in these studies. In the second stage, modelling studies were carried out on premixed methane/air flames at selected mixing ratios. flame length properties were investigated using Zimont.The third stage of this study is to examine the effects of hydrogen enrichment on

premixed flame statistics. All modelling studies were performed with Fluent software and the results were compared with the experimental data. In experimental studies, statistical properties of premixed methane/air and hydrogen doped methane/air flames fixed on a Bunsen-type combustion unit were measured.

2.INTRODUCTION

2.1 Combustion

Increase in heat and production demand causes to use more and more usage in combustion systems. The main component of the natural gas is methane (CH_4). In methane combustion pollutants such as NO_x, CO_2 and unburnt hydrocarbons (UHC) are produced. CO2 is the main contributor of greenhouse gases. Fuel properties, combustion conditions and combustor characteristics determine the qualitative and quantitative pollutant, CO_2 emissions from the combustion chamber and the combustion efficiency [1].

The main goals of reducing pollutant emissions and increasing efficiency can be met by lean burning. However, as fuel/air mixtures are leaned off, the flames can become increasingly difficult to stabilize on a burner or combust. One approach to overcome this problem is to add hydrogen to the fuel. H_2 addition to hydrocarbon fuels can sustain vigorous burning at lower temperatures compared to hydrocarbons [2,3]. Due to that some addition of H_2 can be made to methane combustion to decrease the levels of pollutants.

2.2 Decarbonisation

To prevent the planet from warming 1.5°C above pre-industrial levels, most countries aim to reach net-zero by 2050[4]. Net-zero means that all greenhouse gas emissions produced balanced by an equal number of emissions removed. Achieving this will require rapid decarbonization.

There are two aspects to decarbonization. First, it requires reducing greenhouse gas emissions from the combustion of fossil fuels. This can be done by avoiding emissions by using zero-carbon renewable energy sources such as wind, solar, hydroelectric, geothermal and biomass, which currently account for one-third of global power capacity and electrifying as many sectors as possible. Energy efficiency will reduce energy demand, but increased electrification will increase it, and by 2050 demand of power is expected to be more than double what it is today[4].

Decarbonization is the decreasing carbon dioxide emission thanks to the usage of low carbon power sources.

Decarbonization intends to mention the process of reducing ‘carbon intensity’, decreasing the quantity of greenhouse gas emissions diffused by the burning of fossil fuels.

Nowadays, the reduction of CO_2 gained importance for decarbonization. According to Paris Agreement and UK government reducing CO_2 is necessary to fulfill global temperature standards.

Decarbonization involves increasing the importance of low-carbon energy production and reducing the use of fossil fuels. This contains the utilization of renewable energy sources, in particular wind power, solar power, and biomass.

After prioritizing decarbonization summarized in the Paris Agreement, the UK government has managed to achieve net-zero greenhouse gas emissions by 2050 [4]. After parliament proclaim a climate emergency, the Committee on Climate Change suggested that handle with this net-zero was not only possible but necessary and cost-effective to reach that net zero. Rapid decarbonization becomes more necessary as the transport sector electrifies, increasing the demand for electrical energy. That is why greater energy efficiency becomes a priority to meet emissions targets and improve air quality and global temperature.

2.3 Hydrogen Reactive

The rapid development of the heating industry has exacerbated the energy crises and environmental problems [5]. Methane has great potential and broad application prospects in solving the problem of shortage and environmental pollution [6]. Methane also has shortcomings, such as a low combustion flame velocity and exothermic rate as well as a poor thin combustion capacity [7,8]. Studying hydrogen blending and turbulence intensity is a good way to optimize problems in methane combustion. Hydrogen has characteristics including a high reactivity, a wide combustion boundary, low ignition energy and a much higher combustion rate than that of methane [9,10]. Hydrogen energy is used in the heating industry, aerospace, military and other fields. Hydrogen is one of the most promising clean energy sources [11,12]. Bhasker et al. [13] conducted hydrogen-doping test research on a modified natural gas engine, which proved that the explosion resistance of natural gas in the engine could be improved through hydrogen, meanwhile reducing the emission of CH. Korb B et al. [14] shows that by mixing hydrogen with natural gas, the incomplete combustion loss of natural gas can be reduced, and the combustion stability, as well as the efficiency, can be improved Tomidokoro T et al. [15] studied the characteristics of stratified combustion flame propagation of CH4/air-mixed hydrogen. The rate of stratified flame is higher than that in a uniform mixture. Through experimental and simulation methods, Hu et al. [16] respectively studied the combustion characteristics of methane-hydrogen gas at different equivalent ratios as well as

hydrogen components at room temperature and pressure. They divided the fuel mixture into methane- (hydrogen component was less than 60%) and hydrogen- (hydrogen component was greater than 80%) dominated combustion areas and transition areas (hydrogen component was 60%e80%) according to the laminar combustion rate. Huang et al. [12,17] studied the combustion characteristics of premixed methane/hydrogen in laminar flow. The results show that with the increase of hydrogen ratio, the laminar combustion rate increased, and the maximum laminar combustion rate moved to the direction of mixture concentration. Turbulent combustion is the core of the working cycle of an ignition engine. The turbulence intensity in the combustion chamber directly affects the power of an engine. However, not yet a system has been formed for the research on gas fuel premixed combustion in turbulence, so a reasonable turbulent environment in the combustion chamber is the key to improving heating system efficiency [18].

2.4 Combustion Types:

Combustion can occur in either a flame or nonflame mode, and flames, in turn, are categorized as being either premixed flames or nonpremixed (diffusion) flames. The two classes of flames, premixed and nonpremixed (or diffusion), are related to the state of mixedness of the reactants, as suggested by their names. In a premixed flame, the fuel and the oxidizer are mixed at the molecular level prior to the occurrence of any significant chemical reaction [1].

Non-premixed mode of combustion is traditionally preferred in gas turbine combustors because of safety and stability reasons. Lean Premixed Combustion (LPC) is recently developed along with other methods to achieve lower-level Nox emissions [1,2]. In this mode, the flame is cooler (<1800 K) and thermal NOx is virtually eliminated.

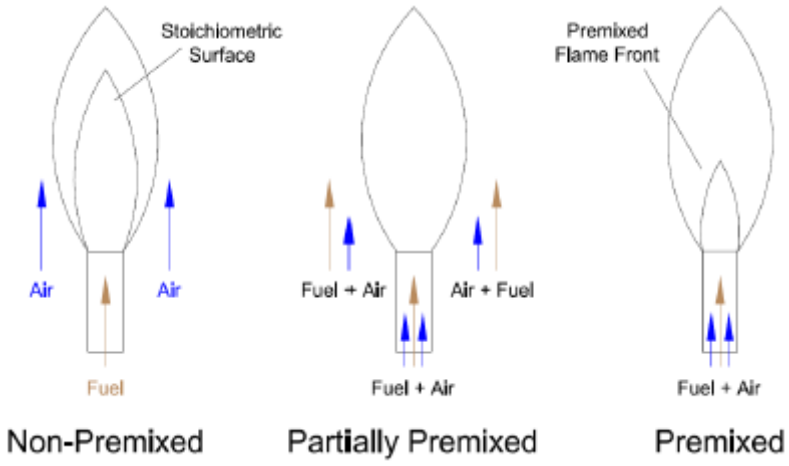

Figure 2.1 Combustion types [20]

In figure 2.1 the types of the combustion are shown. There are three types of combustion[20]:

1. **Non-Premixed Combustion:** Fuel and oxidizer are unmixed before the combustion in non-premixed combustion. In this combustion types the flame can be called as non-premixed or diffusion flames. These types of flames are longer and have lower hot spot temperature than premixed flames.
2. **Premixed Combustion**: Fuel and oxidizer are mixed before the combustion. Premixed flames are shorter and more intense compared with the partially premixed and non premixed flames.
3. **Partially Premixed Combustion**: Some of the fuel and oxidizer mix before the combustion some of the fuel and oxidizeer are unmixed before the combustion. Partially premixed flames have a flame length and temperature distribution between premixed and non-premixed flames.

2.5 Combustion Stoichiometry:

The minimum amount of air needed for the complete combustion of a fuel is called the stoichiometric or theoretical air. Thus, when a fuel is completely burned with theoretical air, no uncombined oxygen is present in the product gases. The theoretical air is also referred to as the chemically correct amount of air, or 100 percent theoretical air. The ideal combustion process during which a fuel is burned completely with theoretical air is called the stoichiometric [28]. The stoichiometric combustion of methane is:

$$CH_4 + 2(O_2 + 3.76N_2) \rightarrow CO_2 + 2H_2O + 7.52N_2$$

For stoichiometric combustion of methane does not include CO, C, H_2, OH, O_2. Equivalence ratio of a stoichiometric combustion is 1. If a combustion that has equivalence ratio lower than 1 there is some excess air in the products of the combustion. Equivalence ratio of a combustion can be found by the formula that is given in below:

$$\phi = \frac{m_{fuel}/m_{air}}{(m_{fuel}/m_{air})_{stoich}} = \frac{m_{fuel}}{m_{air}} * \frac{2 * (2 * M_O + 2 * 3.76 * M_N}{M_{CH_4}}$$

If ϕ>1 the mixture is rich, ϕ<1 the mixture is lean if ϕ=1 the mixture is stoichiometric. Based on that calculation the coefficient of the equation can be found for 0.6 equivalence ratio. The equation that is get for 0.6 equivalence ratio is:

$$CH_4 + \frac{10}{3}(O_2 + 3.76N_2) \rightarrow CO_2 + 2H_2O + \frac{4}{3}O_2 + \frac{37.6}{3}N_2$$

Then, laminar flame speed for different equivalence ratios are got from the reference [1]. In figure 2.2 laminar speed of the methane for different equivalence ratios can be seen. The values of laminar flame speed is taken from there. In 1.05 equivalence ratio the laminar flame speed of methane is the highest. Besides, the higher laminar flame speed causes flasback effect.

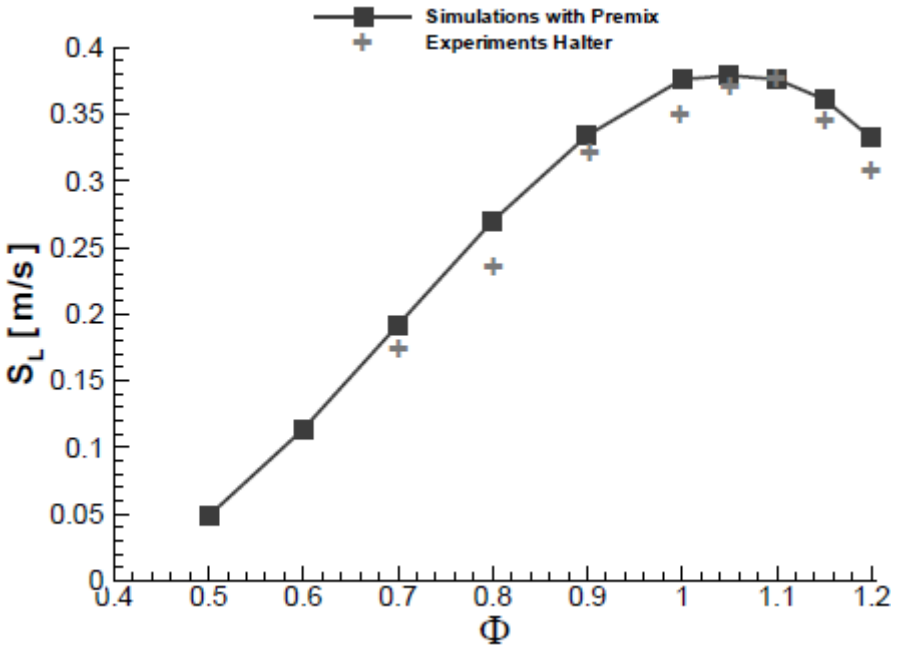

Figure 2.2 Laminar flame speed versus equivalence ratio [1]

2.6 Combustion Products:

In combustion of hydrocarbon fuels, the products of combustion caused to enviromental damage. There are some different combustion products. The main pollutants of the combustion are sulfur oxide and nitric oxide. Sulfur oxide and nitric oxide is considered harmful and increases greenhouse effect.

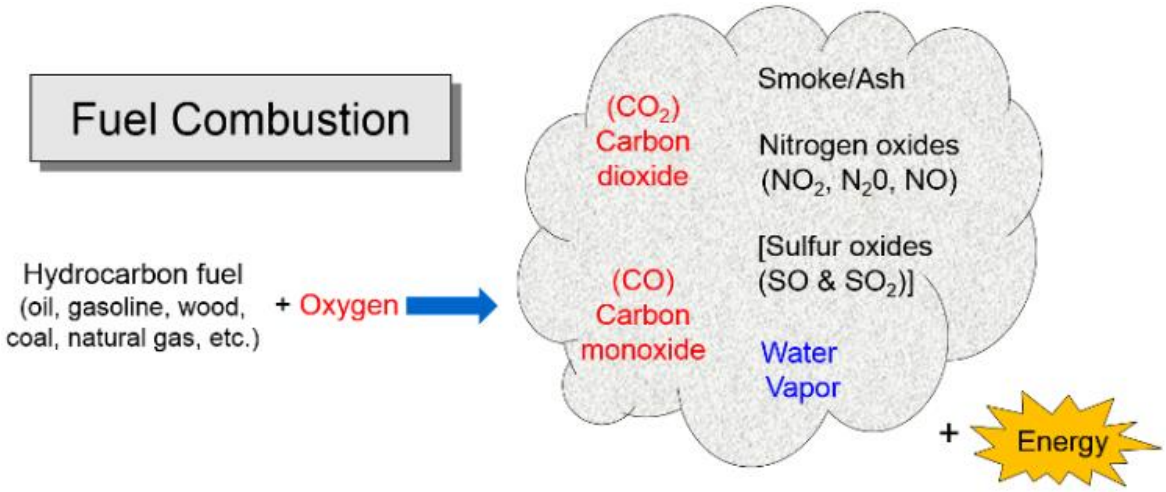

Figure 2.3 Main products of a fuel combustion

The combustion of methane can be considered causes lower harmful effect than from fossil fuels. The emissions of methane-hydrogen mixture has lower flame temperatures. This reason causes decreasing the emissions of combustion. For that reason hydrogen-methane mixture can be used for decreasing emission levels.

2.7 Premixed Combustion Models

2.7.1 Extended Coherent Flamelet Model Theory

The ECFM model solves an additional equation for the flame area density, denoted Σ , which is ultimately used to model the mean reaction rate. The model assumes that the smallest turbulence length scales (Kolmogorov eddies) are larger than the laminar flame thickness, so the effect of turbulence is to wrinkle the laminar flame sheet, however the internal laminar flame profile is not distorted. The increased surface area of the flame results in increased net fuel consumption and an increased flame speed. The range of applicability of the ECFM model is illustrated on the Borghi diagram in Figure 2.4, where the wrinkled flamelets regime is indicated below the Da=1 line. Typical Internal Combustion (IC) engines typically operate in this wrinkled flamelet range.[21]

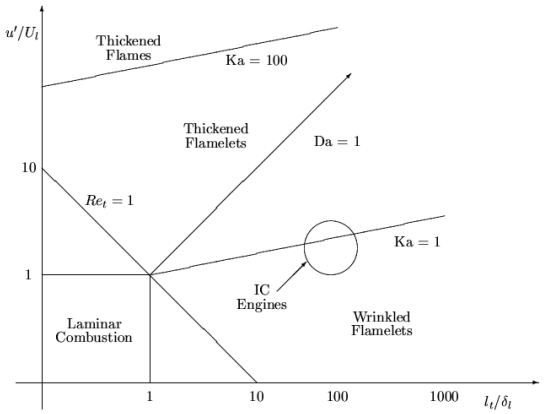

Figure 2.4 Borghi diagram for turbulent combustion

2.7.2 Zimont Model

The regime of thickened flames has been postulated by Zimont [22,23]. He considered the flame in the form of flamelets (similar as in the wrinkled and corrugated flames) but the flamelets are not laminar but rather they are thickened by the turbulence. Borghi [24] gives two consistent explanations of Zimont's concept. The first one assumes that there are turbulent eddies which are small enough to enter the flame front. It results in an increase of heat diffusivity; the flame speed grows and flame thickness increases. Another alternative explanation states that if the size of these small eddies is similar to the flame front thickness, then the curvature of the laminar flame fronts have also a similar size. As a result, the flame front will be thickened even though the reaction zone itself remains thinner than the smallest eddies. In fact it means that the flame front is not thickened but extremely wrinkled. The explanation of Borghi and Zimont are equivalent in fact. In the explanation of Borghi one notes that the interactions of adjacent flame front regions lead to an increase of the heat diffusivity.

3.METHODOLOGY

3.1 Experimental Setup

3.1.1 The High-Pressure Combustion Chamber

The experimental setup of this work includes a high-pressure combustion chamber. This combustion chamber consists of inner diameter of 300 mm and can be operated up to 1 MPa. The chamber has two 600 mm length cylindrical water-cooled sections. In each section of combustion chamber has 4 windows for seeing combustion that will occur. Windows are shown in figure 3.1.

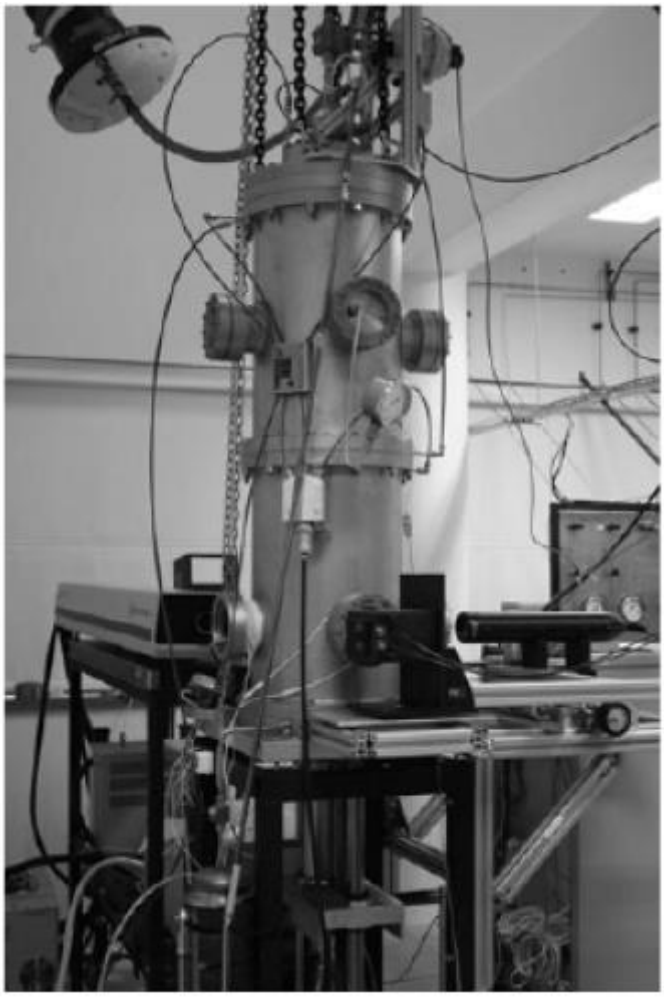

Figure 3.1 High pressure combustion chamber of ICARE [1]

In figure 3.2 the Bunsen burner and its turbulator can be seen. Turbulator of the Bunsen burner consists of a perforated sheet metal. The plate of turbulator has uniformly distributed holes. Mesh distance of the turbulator is 3.5 mm and the diamter of the holes are 2.5 mm. The turbulator is standing 50 mm upstream of the burner to creating turbulence and well mixing of

between methane and air. Besides, a pilot flame is used to burn the premixed mixture that is send to the burner. The pilot flame can be seen in figure 3.2.

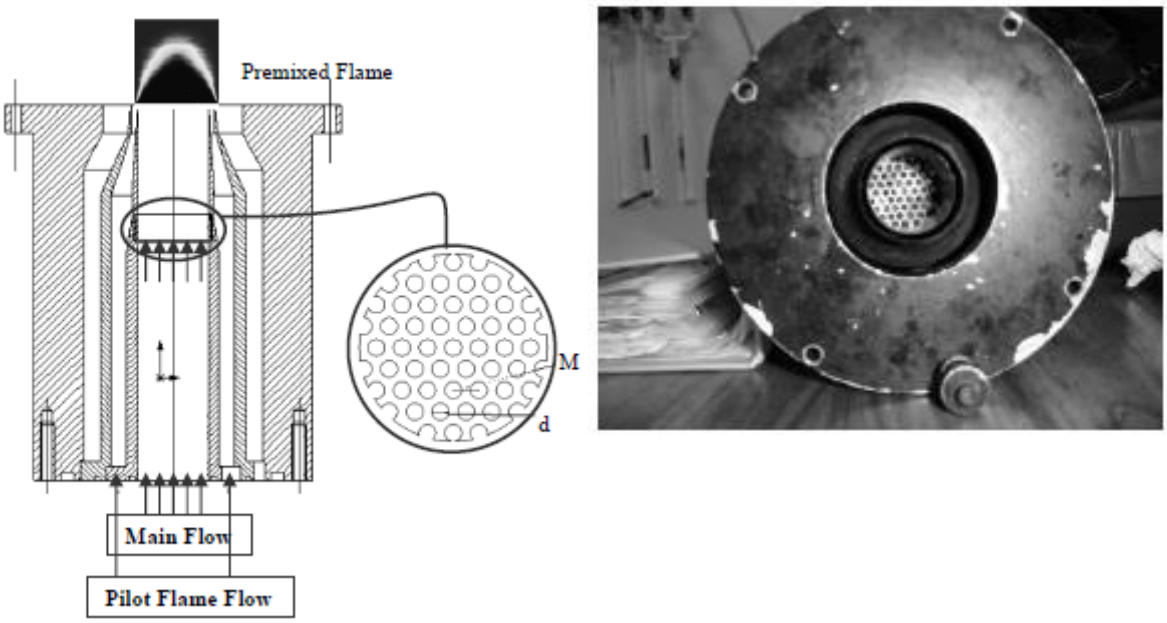

Figure 3.2 The Bunsen burner and their turbulator [1]

3.2 Model Development and Operating Conditions

The cold and reactive flow conditions are selected as in the experiments [25, 26]. Ansys Fluent [21] software is used for numerical studies. A turbulator is used to generate turbulence at the burner exit. A fully developed velocity profile that will be used as the inlet velocity profile for combustion chamber studies is investigated in the burner initially. A combustion chamber geometry is developed in the design modeler of the Ansys. The model is divided into multiple parts to apply different mesh sizes. In the meshing process, the structured fine mesh is applied near the burner exit regions. Smaller mesh size is used along to the axis of the chamber. The bias factor is used to change mesh size at the regions far from the flame. For 2-D cold and reactive flow simulations, a two-dimensional and the axisymmetric chamber model is developed. Coarse meshes are used in regions downstream from the burner exit to reduce computational time.

The grid independent study is done at first. For 2-D and 3-D cold flow, different mesh sizes are used and compared to the Halter [26] and Lachaux [25]. An optimization study is done to obtain the corresponding mass flow rate according to the maximum outlet velocity measured by Halter [26].

The cold flow field is simulated by several k-ε turbulence model variants (RNG, Standard, Realizable). Then, the appropriate model is selected according to the mean velocity distributions along the normalized symmetry axis which is from Halter [26] and Lachaux [25]. Velocity and turbulent kinetic energy have been computed with different k-epsilon models. These results have been validated with experimental data from Halter [26] and Lachaux [25].

The realizable k-epsilon model is used as the turbulence model for the reactive case study. Then, The Zimont model is utilized for simulation with different equivalence ratios. Progress variables are compared with experimental data from Halter [26] and Lachaux [25]. For the reactive case study, SIMPLE method is selected as the solution method and the equation is chosen to be second-order upwind.

3.3 Boundary Conditions

3.3.1 2D Model Boundary Conditions

3.3.1.1 Geometric Modeling

Firstly, the 2D model is drawn in Ansys Geometry module. In figure 3.3 the 2D drawing of the burner can be seen. The half shape of the burner is drawn. The reason of drawing half shape of the burner is Ansys can solve 3D problems as 2D by revolving the shape through on a axis. The cross section of the burner is split on a two symmetric part. Then, the half part of the cross section is drawn into Ansys Geometry module. The dimension of the burner is 300 mm of diameter and 600 mm of height. In figure 3.3 the half of 2D cross section is shown. The dimension of the cross section is 150 mm of height and 600 mm of length. Thus, 2D geometric model of the burner is transferred to the Ansys Geometry module.

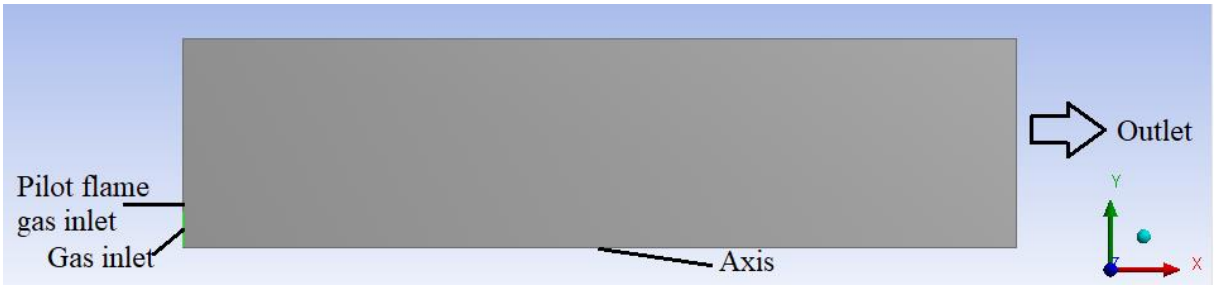

Figure 3.3 Schematic view of the combustion chamber with boundary conditions

3.3.1.2 Meshing:

In meshing part 2 mm face meshing is applied to solve the problem. 21470 nodes are attained by the Ansys Meshing module. Face meshing operator is used to attain mesh to the burner. The face that is selected to assign mesh is half of 2D cross-section of the burner.

The mesh quality of the combustion chamber can be acceptable. The mesh sizing is coarse. Then, the maximum mesh quality is 1 and minimum is zero but in the mesh that is attained by us maximum quality of meshing is 0.99947 and minimum is 0.46789.

3.3.1.3 Numerical Model Setup

After the meshing the numerical setup part had been started. Firstly, general subsection of setup module is opened. In figure 3.4 the general subsection of setup module is shown. The solution is 2D axissymmetric and gravity on x direction. After that, the model's subsection is opened. The model is selected as standart k-e model firstly. Due to this solution is cold flow energy and species are not opened. Besides, when clicking the viscous model part the viscous model selection pop-up menu is opened. In figure 3.5 the viscous model pop-up menu is shown. The k-ε turbulence model and standart model is applied firstly.

In figure 3.6 the materials menu is shown. The related properties of fluids can be changed in this part. In this solution of cold flow, the air is used as fluid of the system.

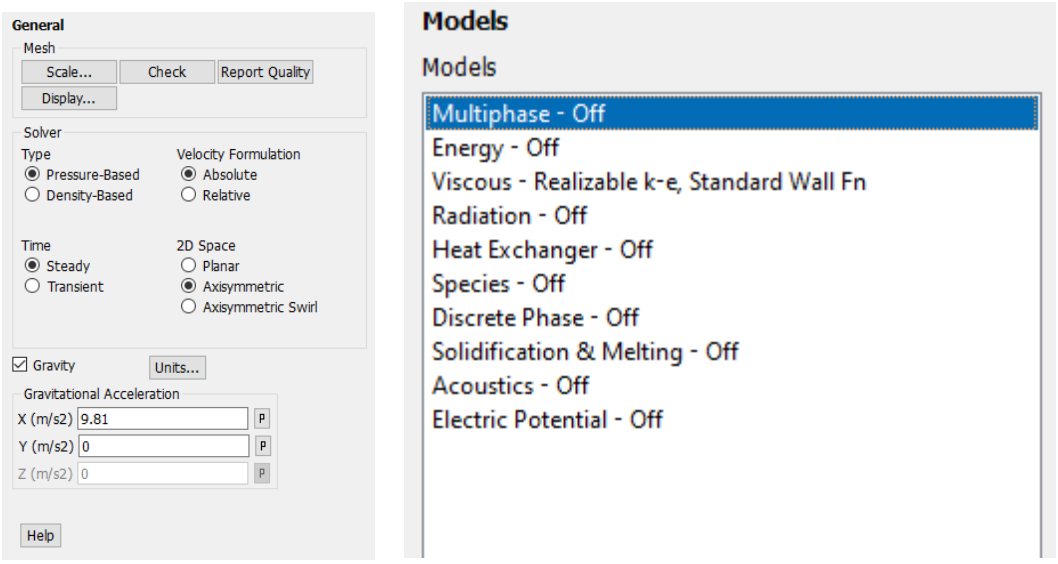

Figure 3.4 General setup and models menu of Fluent

After, the boundary conditions have been applied. The inlet and pilot flame gas velocitiesare defined in this part. The boundary condition's part is shown in figure 3.7. Besides,

the axis of the burner is defined in this part. The inlet velocity that is defined is found by solving velocity of 10 diameter of length of a pipe. The velocity profile that is defined must be fully developed flow. Therefore, a 10 diameter of length pipe flow is solved to get usable velocity profile.

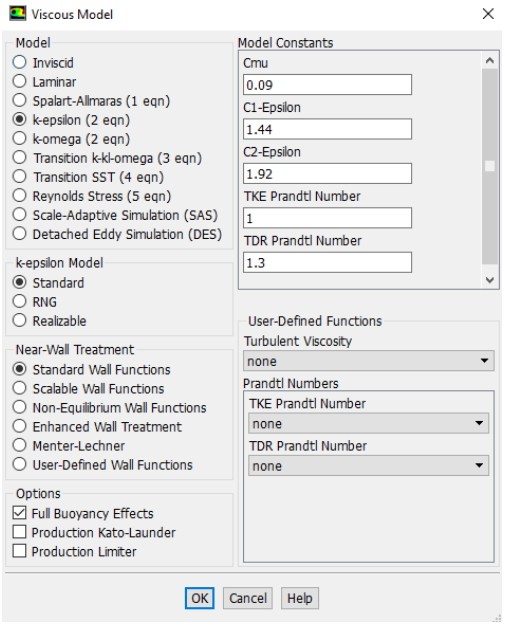

Figure 3.5 Viscous model menu

Then, when the boundary conditions are defined to the Ansys the methods menu is opened. The solution method is selected as coupled. The reason why the coupled method is selected is coupled method can converge faster than other methods. Besides, discretization techniques are selected as second order. The second order discretization gives better results than first order discretization.

After that, the initalization menu is opened. Then, standart initalization is made to initialize the parameters that will found. The residuals are set up to 10^{-5}. Then, the solution menu is opened, and the solution is started.

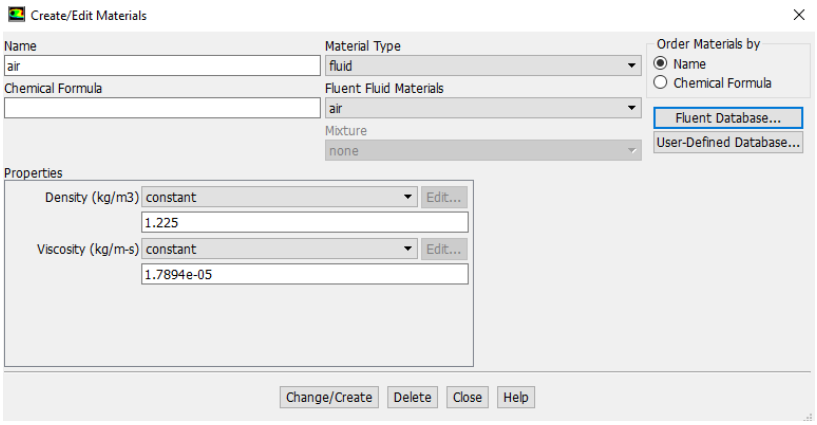

Figure 3.6 Materials menu

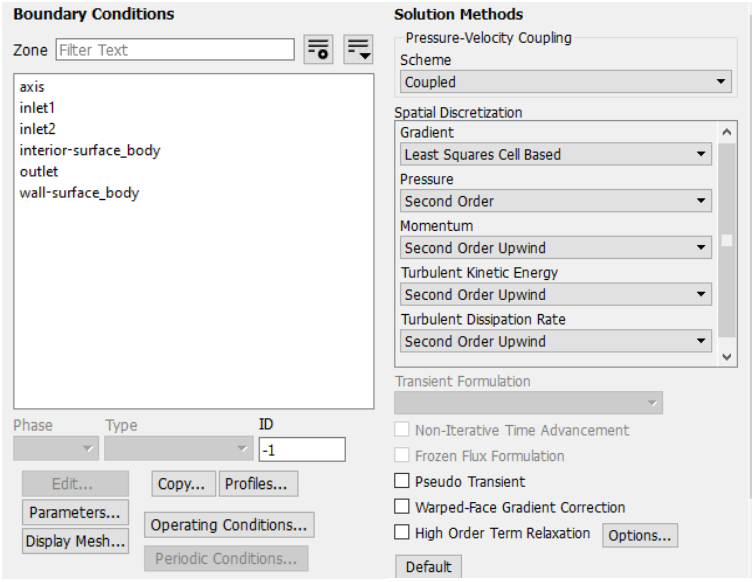

Figure 3.7 Boundary conditions menu and solution method menu is shown respectively

3.3.1.4 3D Model Boundary Condition

In the setup process, the turbulence model is selected as the k-epsilon model Material is chosen as air. The type of inlet boundary is defined as the mass flow rate. When it is entered a value, optimization must be made because the maximum outlet velocity must be 2.51 m/s according to the Halter experiment and Lanchaux experiment. As shown in table 4.1, the mass flow rate is chosen as 0.000111 kg/s according to maximum velocity.

3.4. 3-D Velocity Profile

A cylindrical model with a diameter of 0.025 meters and a length of 1 meter is used to obtain a fully developed velocity profile. As seen in figure 3.8, it represents a turbulator for getting velocity profile.

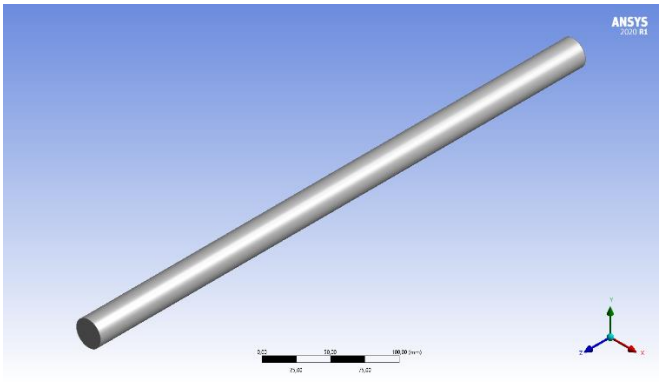

Figure 3.8 Cylindrical Model

In the meshing process, a structured mesh is utilized for obtaining more accuracy. To get a structured mesh, the mesh method is inserted as multizone. Therefore, edge sizing is inserted by choosing a type which is the number of divisions. The number of divisions is adjusted to get a high-quality mesh as seen in figure 3.10. At the end of the meshing process, the number of nodes is 458481.

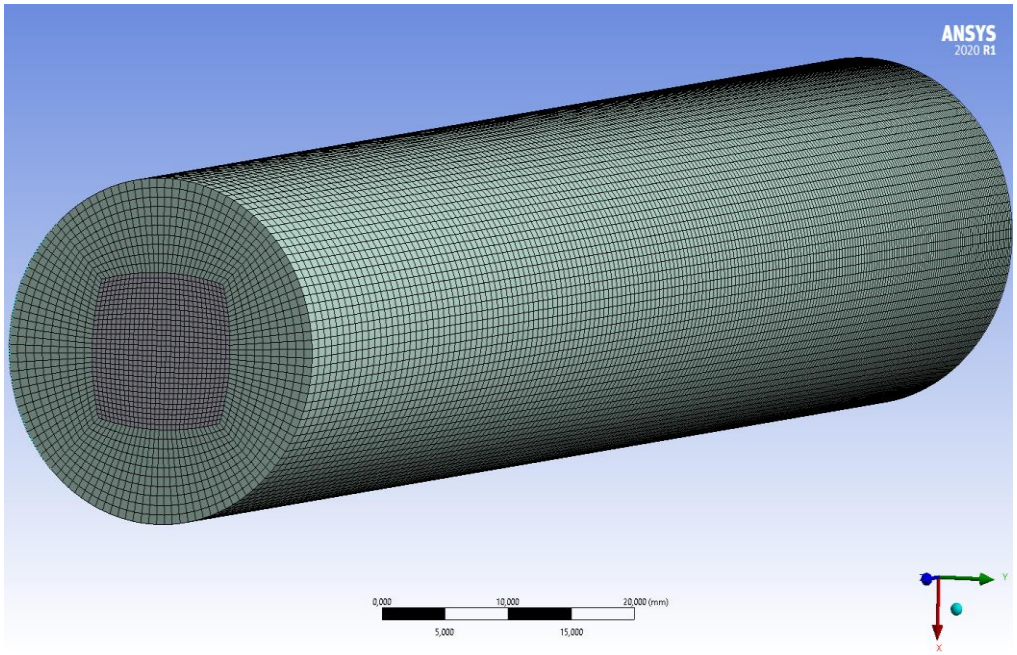

Figure 3.9 Mesh Structure

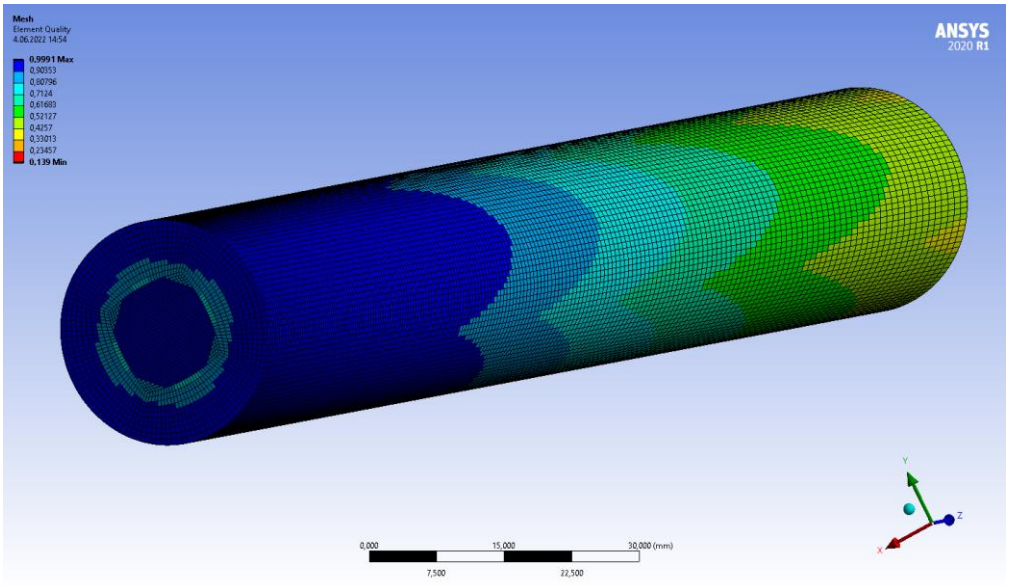

Figure 3.10 Element Quality

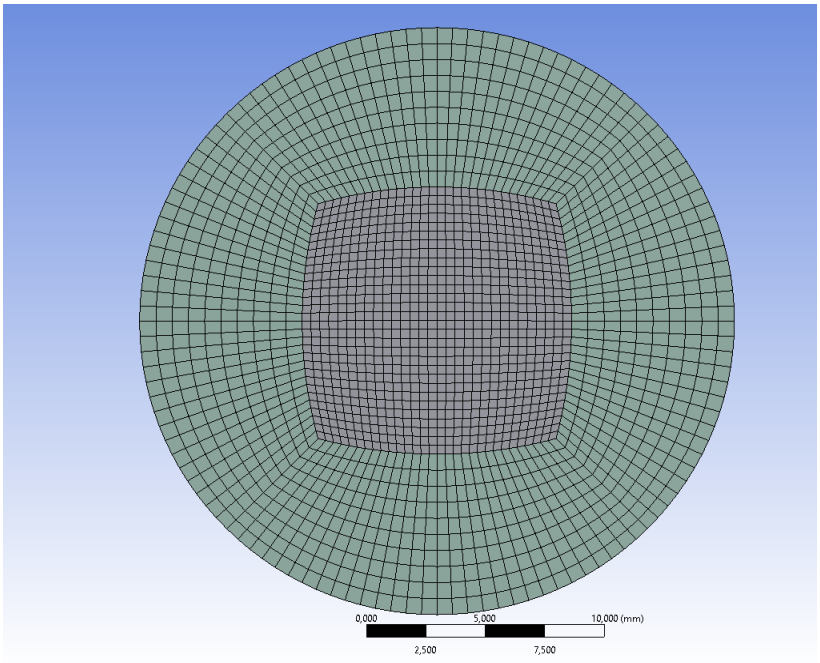

Figure 3.11 Detailed input mesh structure

Table 4.1 Maximum outlet velocity with the mass flow rate

Mass Flow Rate m $(\frac{\dot{kg}}{s})$	Maximum Velocity in Outlet $(\frac{m}{s})$
0.0012247	2.7387
0.001120	2.5372

0.000111	2.5178
0.00110	2.4984

After deciding on the mass flow rate, the velocity profile is obtained as seen in figure 4.22

4.4.2. 3D-Combustion Chamber Reactive Flow Setup

4.4.2.1 Geometric Modeling

In this process, the turbulent model is chosen as k-epsilon and it consists of 3 parts which are standard, RNG, and realizable. 3 methods are selected to compare each other, and experiment values are named Halter and Lanchaux. As seen in figure 4.22, the velocity profile which is obtained in the previous part is defined as the figure. The couple is chosen as a solution method and the initialization method is defined as the standard initialization which is computed from inlet.

Burner is designed according to Halter and Lachaux's experiment. As shown in figure 3.12, It consists of four parts because it is easier to control in the meshing process.

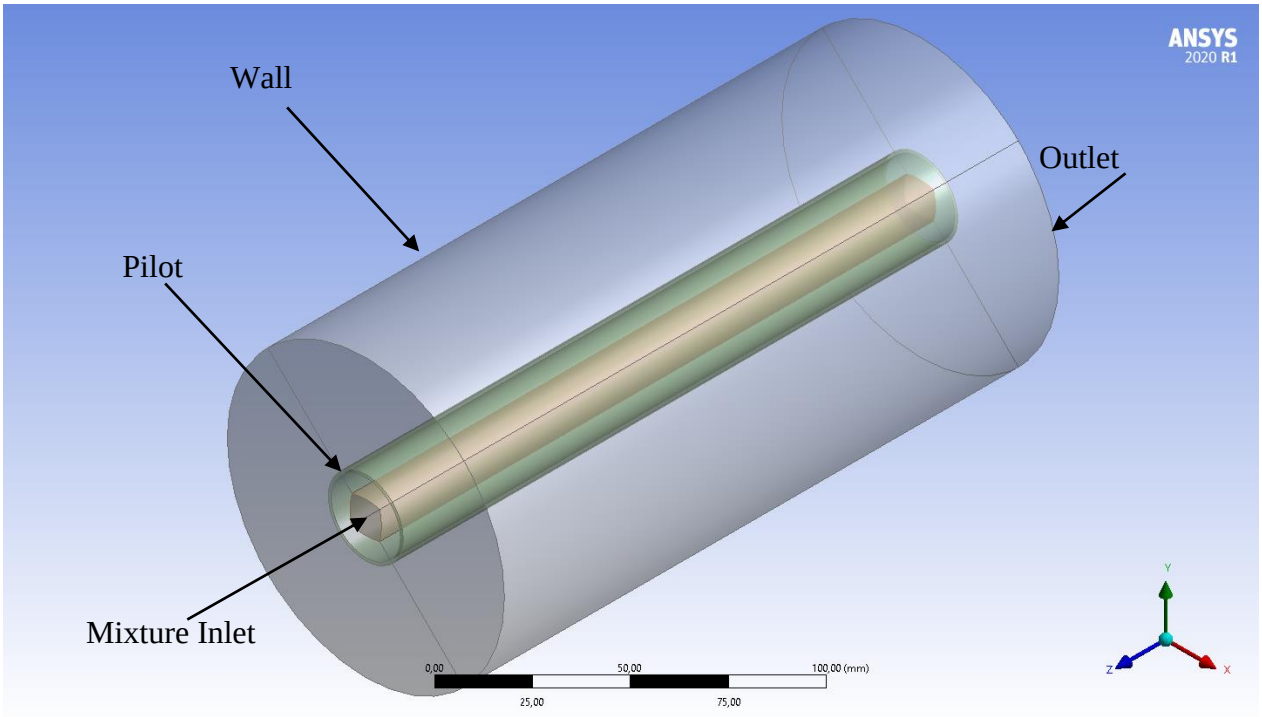

Figure 3.12 Geometry of burner model

In the meshing part, part of the mixture inlet is applied smaller mesh size to obtain good results. To do this, mesh sizing is inserted, and type is chosen as the number of divisions with bias factor 4. As shown in figure 3.13, the meshing size is more frequently as it goes from the center to the edges. Mesh quality varies between 0.7-0.99 in the centre of the flow. Mesh quality decreases farther from the centre. The number of nodes is 1278561.

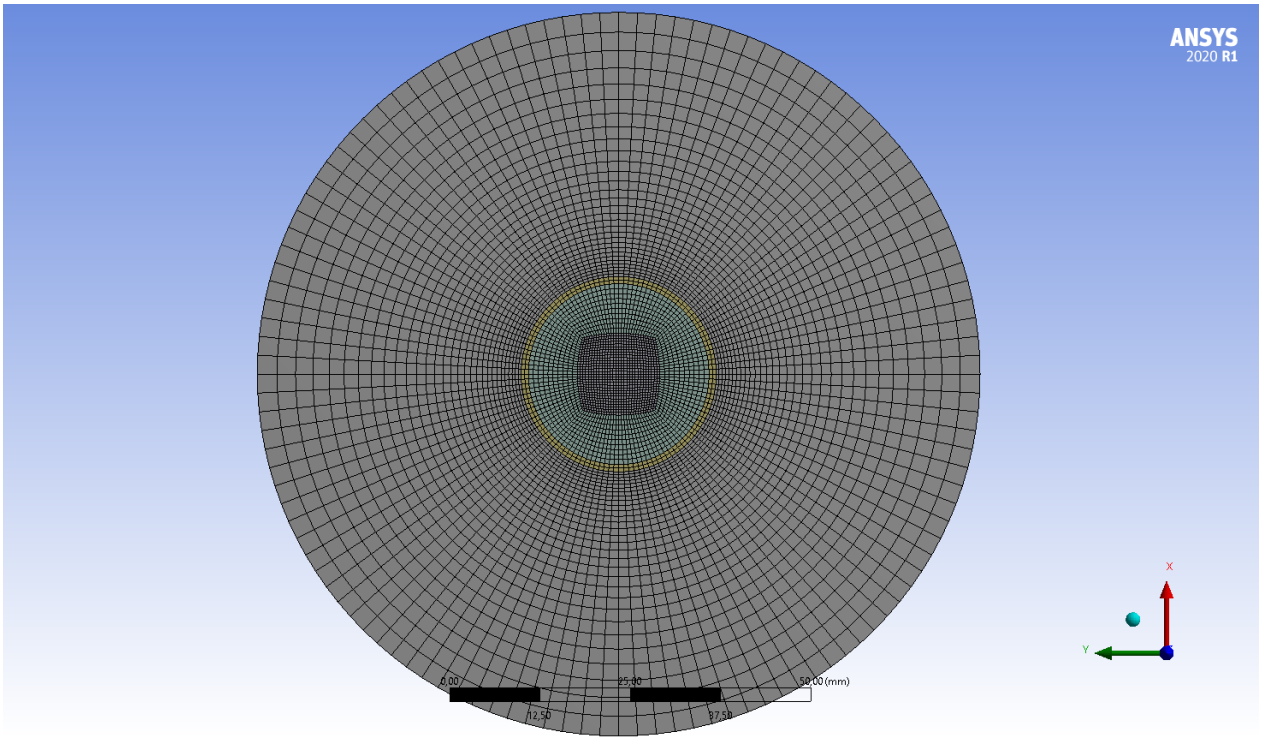

Figure 3.13 The mesh structure of the combustion chamber

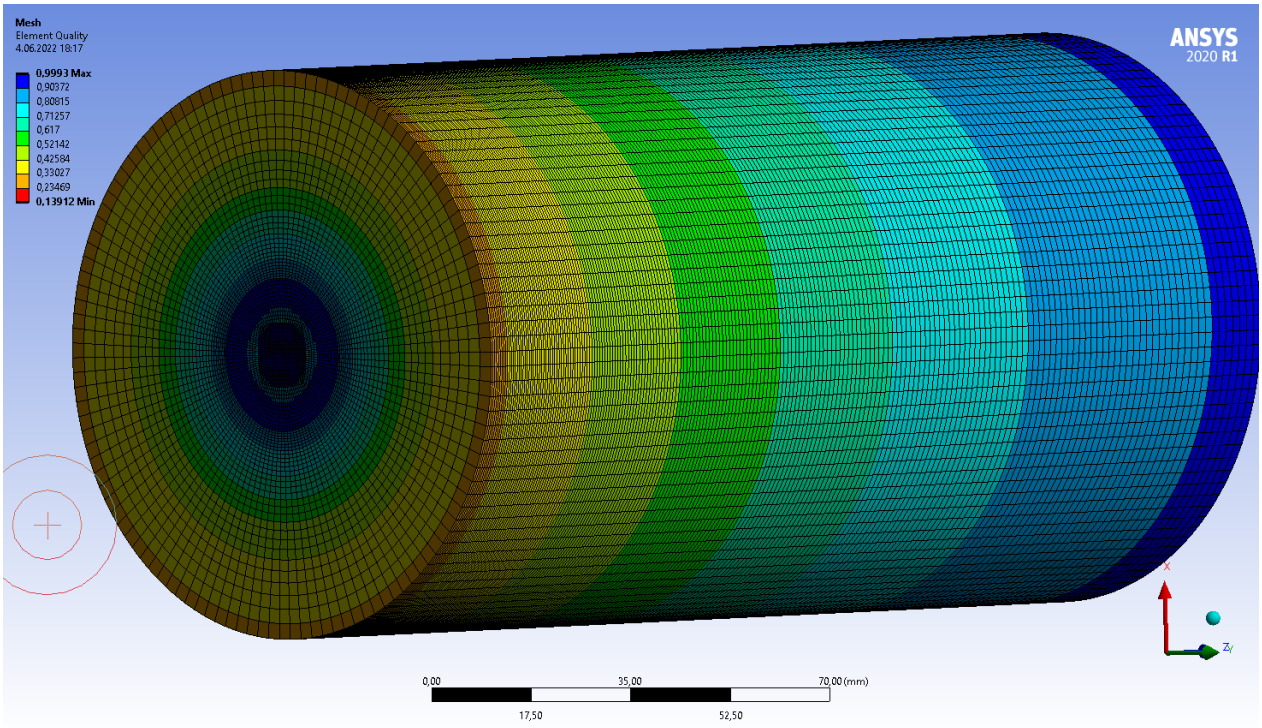

Figure 3.14 Mesh quality of combustion chamber

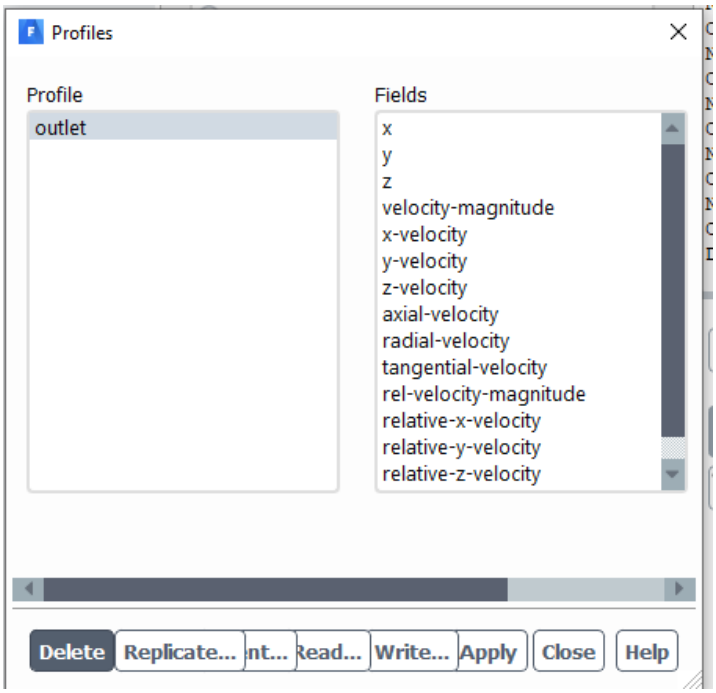

Figure 3.15 Import of fully developed velocity profile

After the solution, the solution converges in different iterations as shown in table 4.6. The continuity value reaches 10^{-6} in all models.

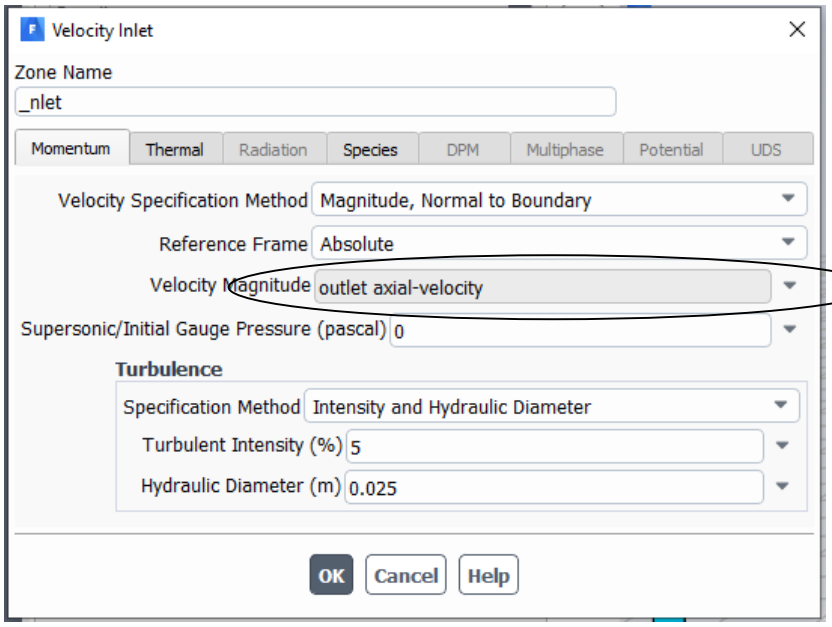

Figure 3.16 Definition of boundary conditions for inlet velocity

3.4 Governing Equations

The conical jet flow becomes turbulent mainly by the effect of the turbulence grid used in burner section and the shear forces between the main flow and the surrounding air inside the studied combustion chamber. Developed turbulent flow field is modeled by several variants of the k-ε turbulence model. In this model, the flow field is described by Favre-averaged Navier-Stokes equations in the conservative form. Besides the continuity and momentum equations two more scalar transport equations are solved which are defined in the following form in Fluent [21] .

$$\frac{\partial \rho k}{\partial t} + \frac{\partial}{\partial x_i}(\rho k u_i) = \frac{\partial}{\partial x_i}\left((\mu + \frac{\mu_i}{\sigma_k})\frac{\partial k}{\partial x_i}\right) + G_k - \rho\varepsilon \tag{3.1}$$

$$\frac{\partial \rho \varepsilon}{\partial t} + \frac{\partial}{\partial x_i}(\rho \varepsilon u_i) = \frac{\partial}{\partial x_i}\left((\mu + \frac{\mu_i}{\sigma_\varepsilon})\frac{\partial \varepsilon}{\partial x_i}\right) + C_{\varepsilon_1} G_k - C_{\varepsilon_2}\rho\frac{\varepsilon^2}{k} \tag{3.2}$$

The equation (3.3) describe turbulent viscosity

$$\mu_t = \rho C_\mu \frac{k^2}{\varepsilon} \tag{3.3}$$

3.5 Propagation of the Flame Front

In many industrial premixed systems, combustion takes place in a thin flame sheet. As the flame front moves, combustion of unburnt reactants occurs, converting unburnt premixed reactants to burnt products. The premixed combustion model thus considers the reacting flow field to be divided into regions of burnt and unburnt species, separated by the flame sheet. The flame front propagation is modeled by solving a transport equation for the density-weighted mean reaction progress variable, denoted by c[27]:

$$\frac{\partial}{\partial t}(\rho c) + \nabla(\rho \vec{v} c) = \nabla\left(\frac{\mu_t}{Sc_t}\right) + \rho S_c \tag{3.4}$$

Where

C= mean reaction progress variable

Sct= turbulent Schmidt number

Sc= reaction progress source term (s^{-1})

The progress variable is defined as a normalized sum of the product species,

$$c = \frac{\sum_{i=1}^{n} Y_i}{\sum_{i=1}^{n} Y_{i,eq}} \tag{3.5}$$

Where

n= number of products

Y_i= mass fraction of product species i

$Y_{i,eq}$= equilibrium mass fraction of product species i

Based on this definition, c=0 where the mixture is unburnt and c=1 where the mixture is burnt:

c=0: unburnt mixture

c=1: burnt mixture

The value of c is defined as a boundary condition at all flow inlets. It is usually specified as either 0 (unburnt) or 1 (burnt).

$$\rho S_c = \rho_u U_t |\nabla_c| \tag{3.6}$$

where

$\boldsymbol{\rho_u}$= Density of unburnt mixture

$\boldsymbol{U_t}$=Turbulent flame speed

3.6 Numerical Studies

Firstly, axisymmetric and 2D model of the high-pressure combustion chamber is developed. Then, mesh sizing is applied to this model. Basically, the mesh sizing is kept densely in the part that combustion occur. The mesh sizing in the part that combustion products will go out is kept coarse. After the meshing part is done, the cold flow is solved by the Ansys Fluent software. Before doing calculation of cold flow the inlet velocity profile of the burner is solved by a new geometry. In the work that will be done the turbulator will not use. Therefore the velocity profile of the inlet is found by solving a 25 mm of diameter and 10D or 250 mm of length body The velocity results are get from the Ansys Fluent. The results of velocity profile are used to defining the velocity inlet.

After that, the grid independent solution is made on cold flow. The mesh size and type of meshing is selected on this work of grid independent solution. Different mesh combinations are tried on cold flow and the results of cold flow are compared with Experimental results of Halter [26] and Lachaux [25].

After the grid independent soluiton is made different model solution is started. K-ε, RNG and Realizable model are tried in cold flow. The results that are get from the three are compared with experimental data from Halter[26] and Lachaux[25]. The model that is in good agreement with experiments is selected to use in the next part of the work.

In the reactive flow of the work, the model selection and the mesh type and size selection on the cold flow is used. Viscous model selection and mesh selection that is found in cold flow have been carried to reactive flow. In addition to this in reactive flow the material properties of the mixture are defined. The material properties and flame speed of the methane-air mixture with different equivalence ratios are taken as in Ref. [25,26]. In Reference [1] the required flame properties were calculated with Chemkin software with GRI Mech3.0 chemical mechanism. Species model is selected as Zimont model with laminar flame speed constant of 0.52.

4.RESULTS

4.1 COLD FLOW MODEL SETUP:

4.2 COLD FLOW TURBULENCE MODEL SELECTION

Three variants of the k-e turbulence models are used to solve the flow using Fluent. First is standart method, second is RNG method and the last method is Realizable. In essence of the three method give similiar results but there is some different. The results that are get by the three method can be compared with the Experimental results of Halter and Lachaux. In this part the methods of the viscous model will be compared.

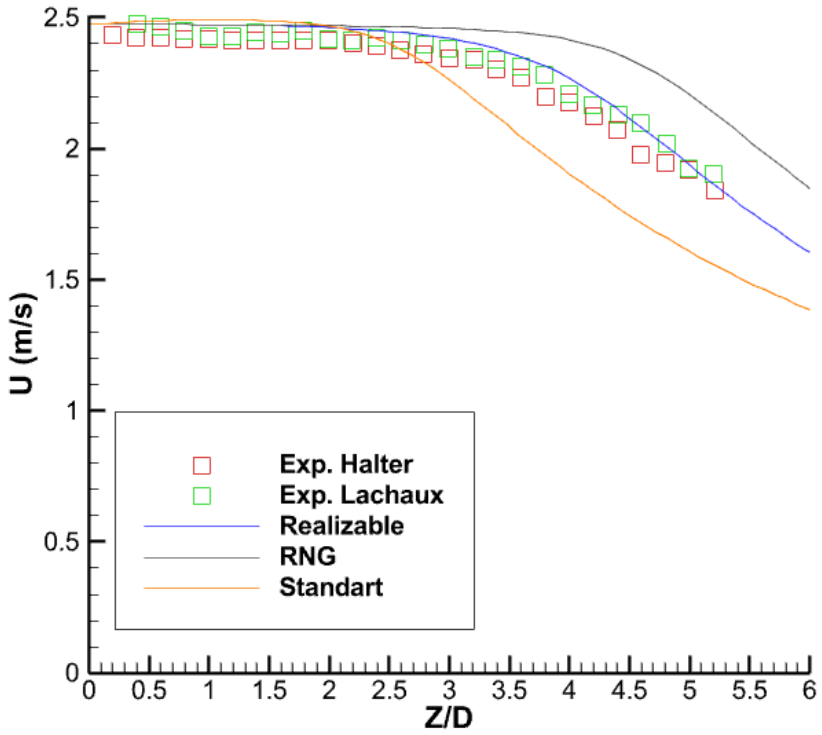

Figure 4.1 The predicted Axial Velocity profiles with different k-e model variants versus normalized axis

The velocities at the burner esit are computed by the Ansys Fluent software. Then, the results of the three methods are get. After getting the axial velocities at the axis of the burner the CFD results of the cold flow and the experimental results of the Halter and Lachaux are drawn for comparison in TECPLOT Software. When, the methods are compared the Realizable method is similiar to the results that are measured by the epxeriments of Lachaux[25] and Halter[26]. The normalized, z/D, velocity graph can be seen in figure 4.1. Besides, in figure 4.2 the normalized z/D-velocity graph can be seen. The normalized Z/D-velocity graph is get for

comparing results of the three methods quantitavely. Then, the Realizable method is decide to use for the further part of the solutions.

The residuals are shown in figure 4.3. The solution had finished when the all residuals lower than 10^{-5}.

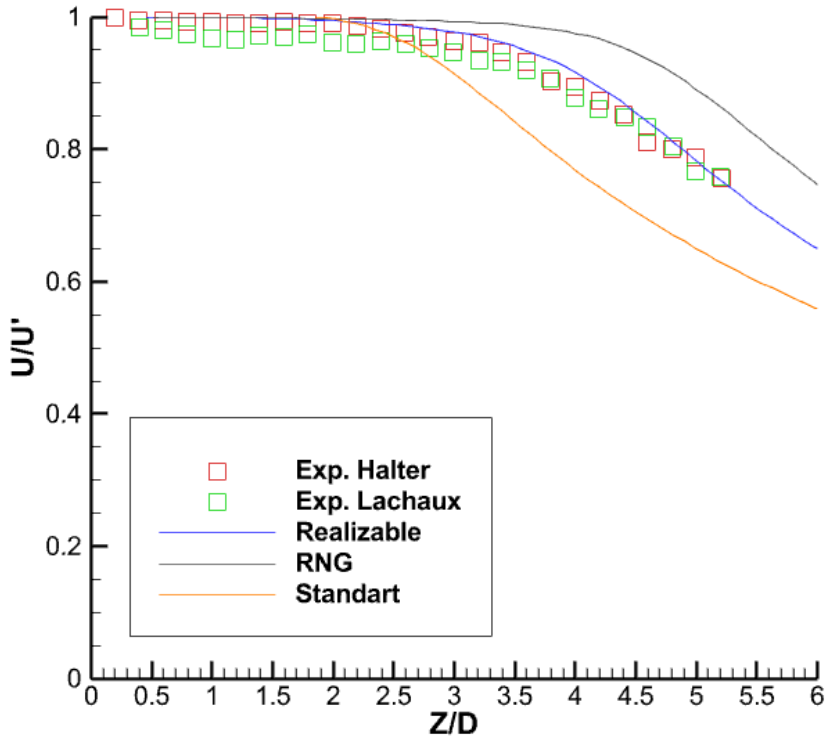

Figure 4.2 Normalized Z/D-Velocity Graph

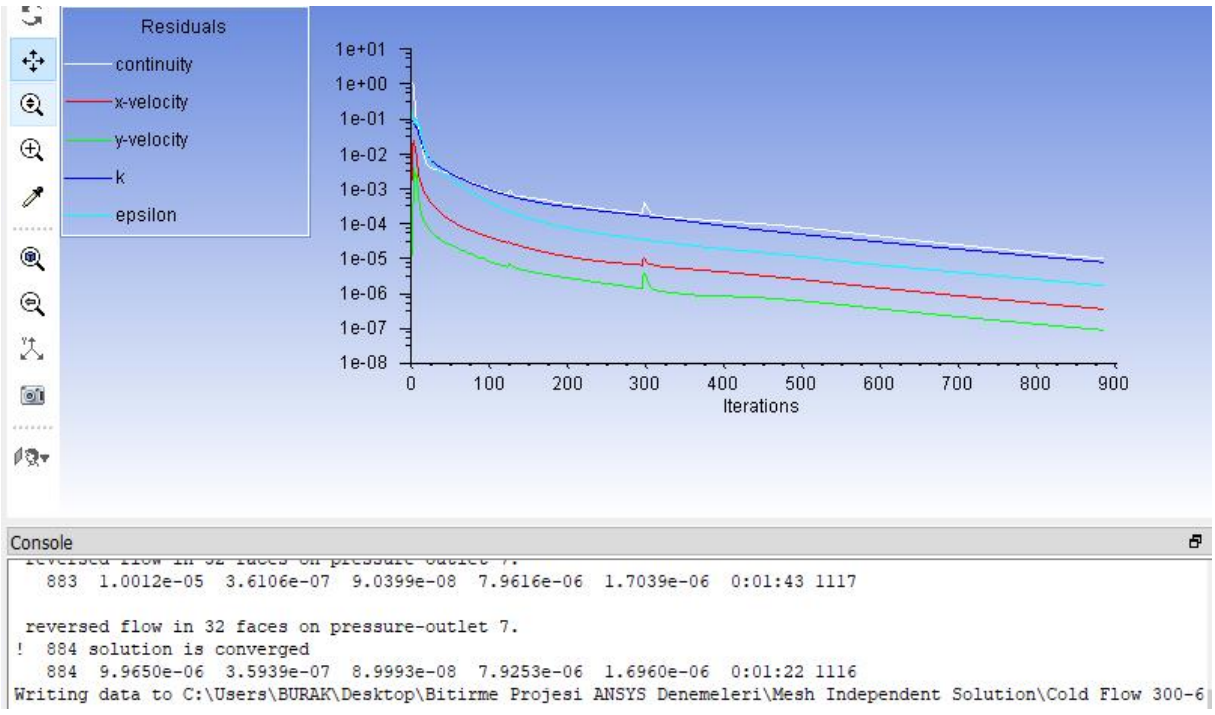

Figure 4.3 Residuals that is happened when the solution had finished

4.3 COLD FLOW GRID INDEPENDENT SOLUTION:

The turbulence model is selected as Realizable k-e model. Then, the mesh size of the burner is selected by comparing the results that are get by the Ansys. The different mesh size can be tried to solve velocities that are happened on the burner by the Fluent software. Then, the different mesh sizes are selected as 5,2,1 and 0.75 mm. The mesh size of the burner can be chosen between 5,2,1 and 0.75 mm of sizing. The number nodes are shown in table 4.2.

Table 4.2 Mesh sizing number of nodes table.

	Mesh Sizing			
	5 mm	2 mm	1 mm	0.75 mm
Number of nodes	3390	21470	90478	158856

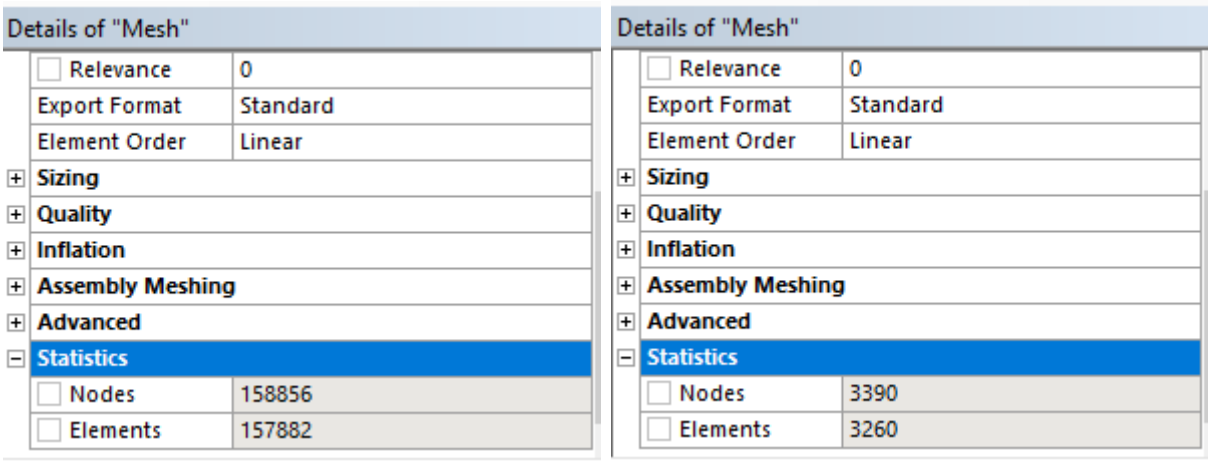

Figure 4.4 The number nodes of 0.75 mm mesh sizing and 5 mm mesh sizing respectively

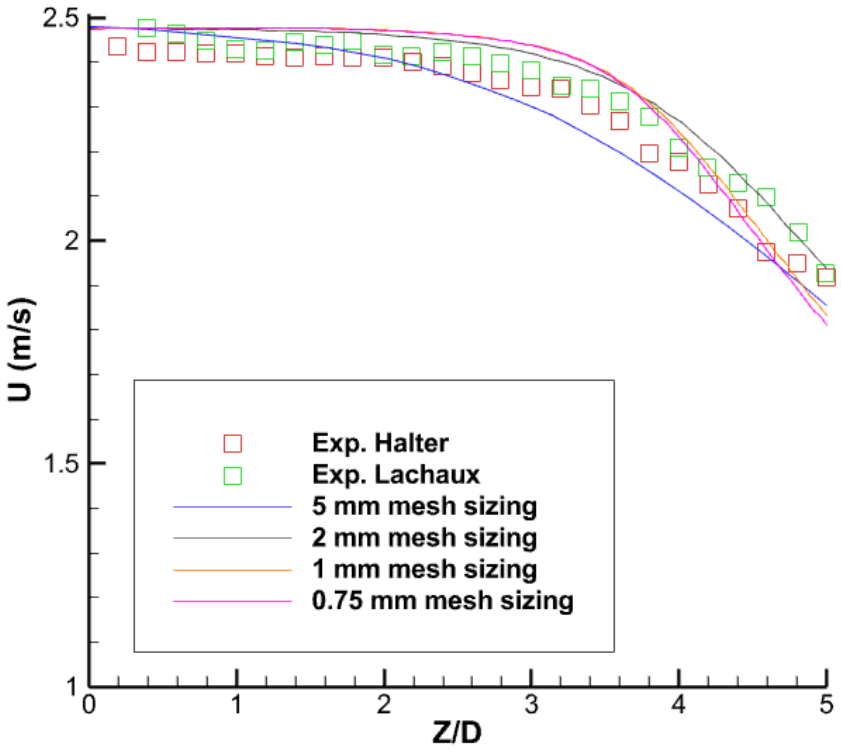

Figure 4.5 The Z/D-Velocity graph with different mesh sizing

In figure 4.5 the velocity-Z/D graph is shown. The graph compares the results that are get from the experiments of Halter and Lachaux and results from Ansys software with different size of meshes. In figure 4.5 shows related results but best mesh sizing can not appear easily. For that reason, velocities divided by its maximum value. Then, the normalized velocity-Z/D graph is drawn. In figure 4.6 normalized velocity and Z/D graph is shown.

In figure 4.6 it can be shown how the velocity results affected by different mesh sizing. The results that are get by the Ansys Fluent software with different mesh sizing are similar to each other.Altought results that are get by Fluent software are similar to Experimental results of Halter and Lachaux. The 1 mm mesh sizing is selected to get more accurate results. In figure 4.7 1 mm mesh sizing normalized velocity result and Z/D graph can be shown. The 1 mm mesh sizing is enough to get close velocity value from experiments of Halter and Lachaux. The 1 mm mesh sizing and Realizable method will be used to analyse premixed combustion in 2D analysis.

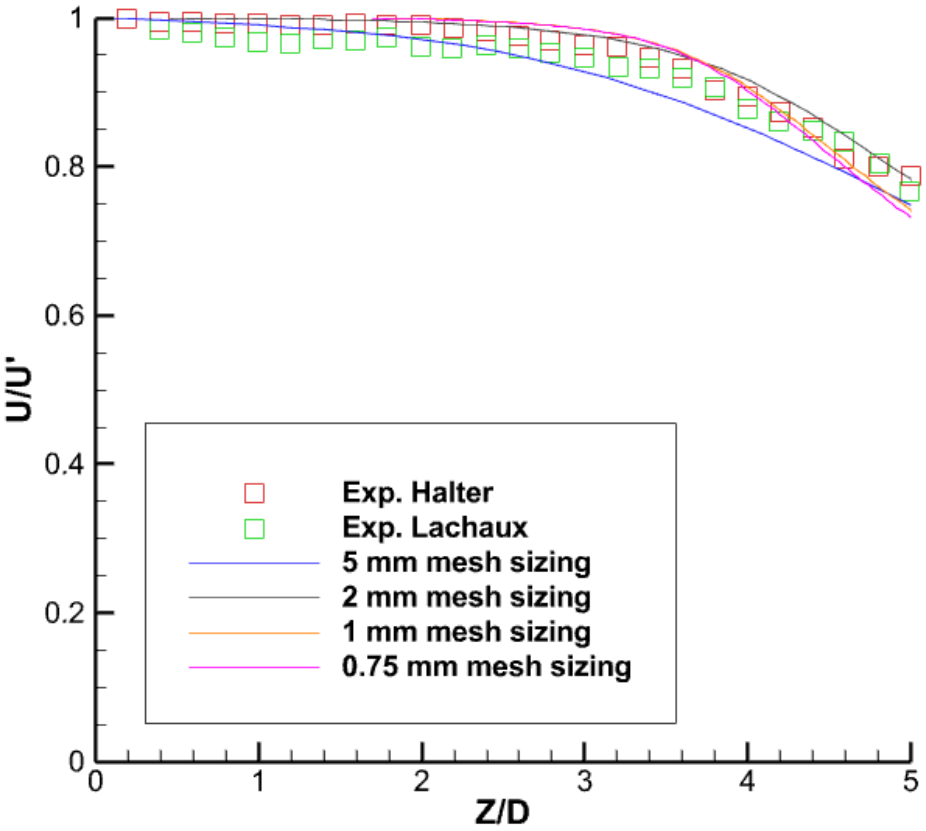

Figure 4.6 The Z/D-Normalized Velocity graph with different mesh sizing

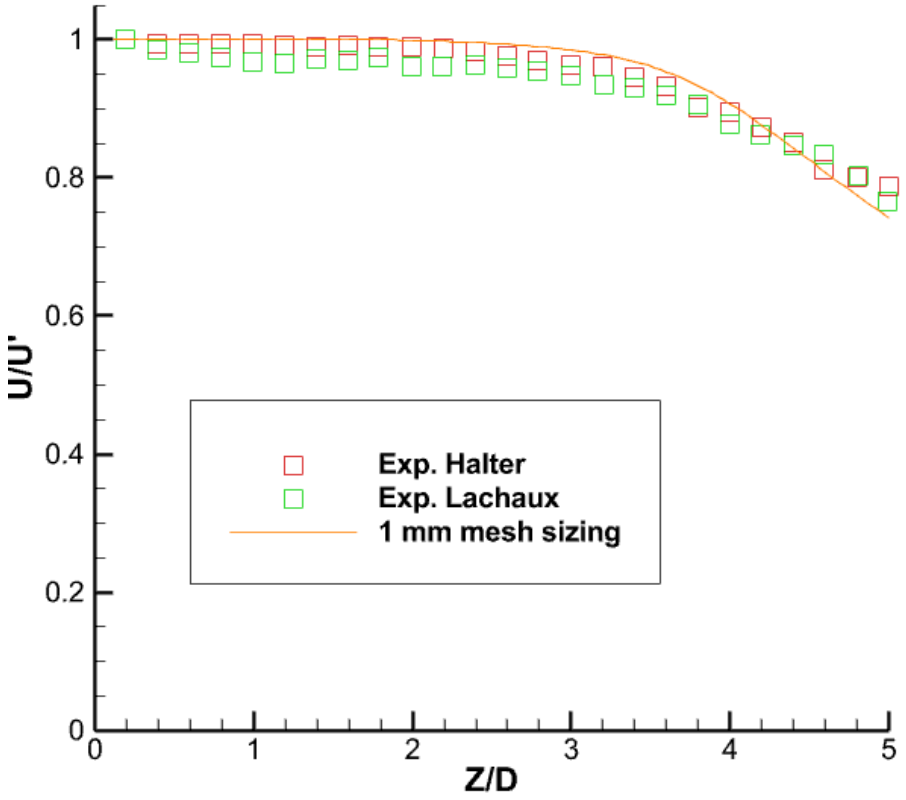

Figure 4.7 The Z/D-Normalized Velocity graph with 1 mm mesh sizing

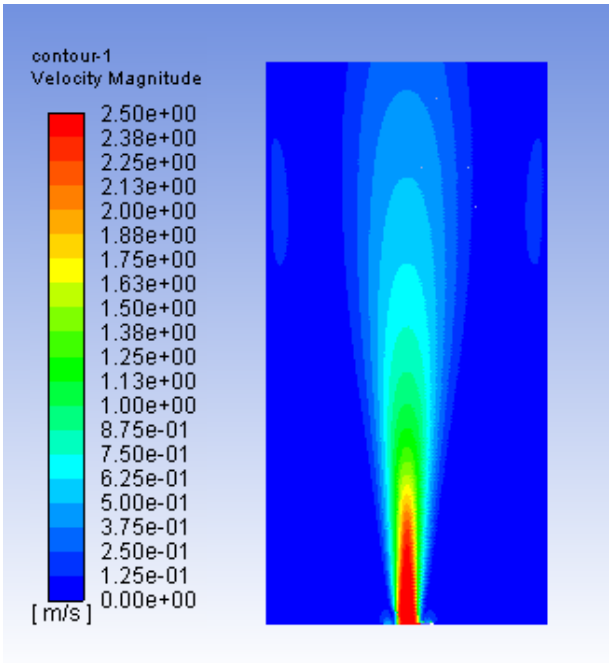

Figure 4.8 Velocity contour of 1 mm mesh sizing

4.4 REACTIVE FLOW:

4.4.1 2D Reactive Flow:

4.4.1.1 2D Reactive Flow Setup:

In the project the combustion process is splitted into two parts as 2D and 3D. In 2D combustion process meshing part had not take more time. In cold flow the mesh size is selected as 1 mm. In 2D combustion part the 1 mm mesh sizing is applied to burner. The half of the cross-section of the body is taken in 2D combustion. Ansys Fluent software solves the 3D problems as 2D. A symmetry axis is defined into the Ansys Fluent software. Then the software revolves the 2D body. Then, a 3D body is constructed. Therefore, the solution of a 3D problem can solve by solving 2D problem with axisymmetric method.

The half cross-section of our body is transferred to the Ansys Fluent software. Then, the selected mesh of 1 mm is applied to the burner that will be analysed. There is no mesh quality problem in 2D solution.

After meshing process, the setup part is opened. When the setup part is opened firstly general subsection had seen in setup part. The general subsection includes time, 2D space, gravity etc. The gravity is adjusted as 9.81 m/s^2 in x direction. Then, the axisymetric option is

selected in 2D space part. Then, in viscous model menu k-epsilon model and realizable submodel is selected. Due to Realizable submodel gave appropriated results on cold flow in 2D premixed model solution the Realizable submodel is selected. In figure 4.9 the viscous model menu and general menu is shown. Then, in figure 4.10 species model menu is shown. In this menu the combustion model is selected. Premixed combustion model is selected. Besides, model option is selected as non-adiabatic model, C equation and zimont model.

After selecting the viscous model, the material of methane is defined. In figure 4.11 the material properties of equivalence ratio of 0.7 can be seen. Then, the boundary conditions are defined as same as in cold flow. But in premixed combustion progress variables are defined to the inlet and outlet ports. Progress variables are defined as 0 for fresh mixture 1 for burned mixture. Then, solution method menu is opened, and second order Coupled method is selected to solve the problem

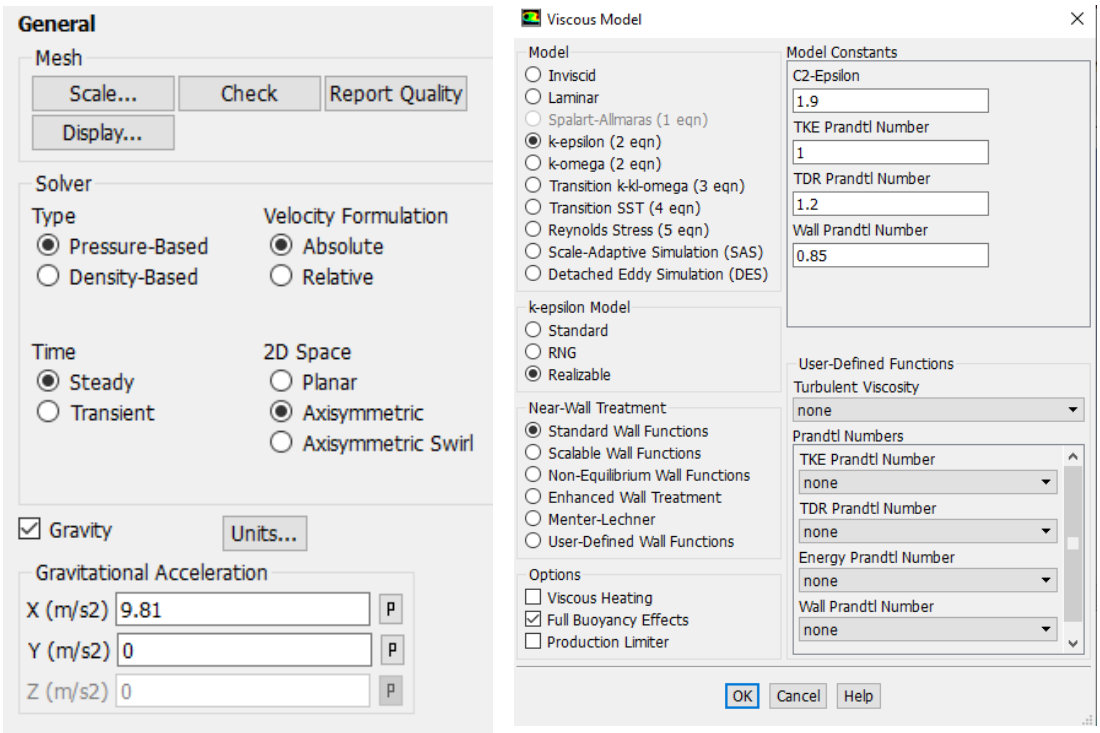

Figure 4.9 General and viscous model menu

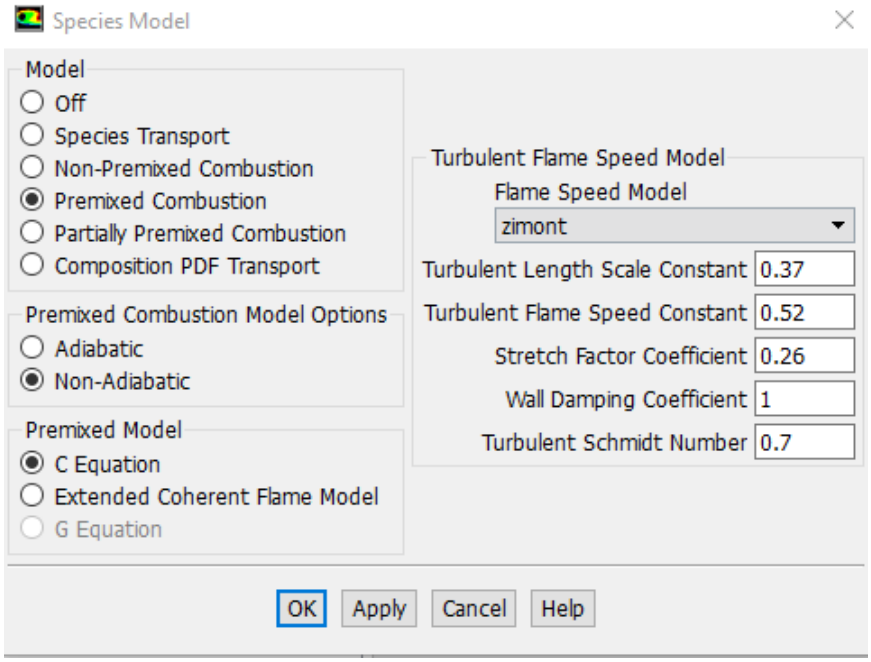

Figure 4.10 Species model menu

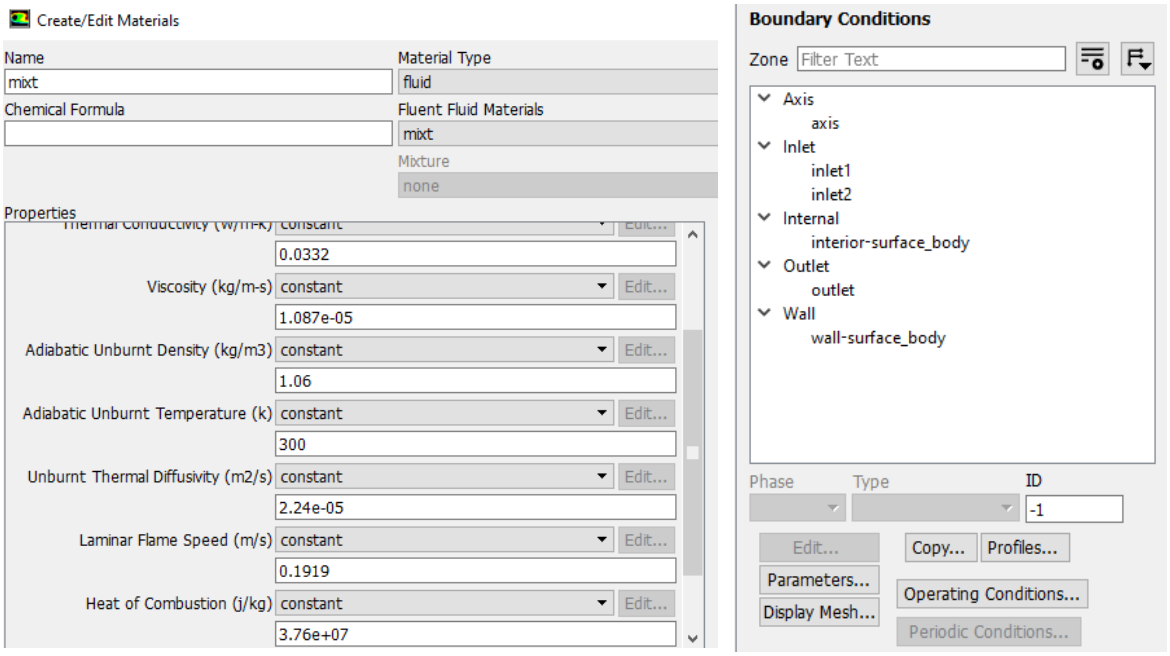

Figure 4.11 Material menu and boundary condition menu respectively

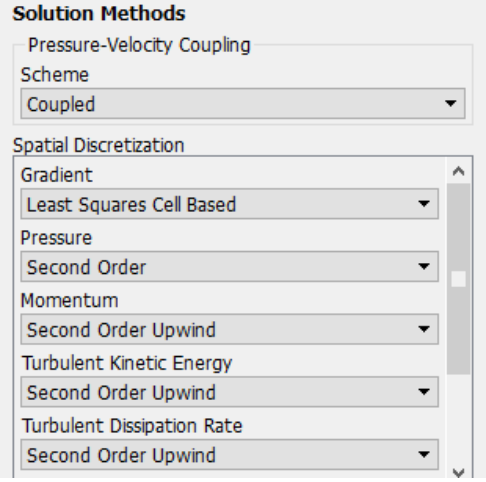

Figure 4.12 Solution method menu

4.4.1.2 Material Properties:

The 2D premixed combustion is solved via Ansys Fluent software. The solution is made for 0.6, 0.7 and 0.8 equivalence ratios for methane. For different equivalence ratios the material properties change. For that reason, the heat of combustion, density of mixture values is found by an Excel file. In table 4.3 the densities of the mixture are shown. In table 4.4 the coefficients of methane combustion are shown. In table 4.5 the heat of combustion of methane for different equivalence ratios of 0.6,0.7 and 0.8. In figure 4.13 the laminar flame speeds of related equivalence raitos can be seen.

Table 4.3 Density of mixture

Reactants		
CH4	Air	H2
0.8	3.20833	0.2
	Density	1.06279
ER=0.6	1.09003	kg/m^3
ER=0.7	1.07785	kg/m^3
ER=0.8	1.06271	kg/m^3
%5 H2	1.08322	kg/m^3
%10 H2	1.07641	kg/m^3
%20 H2	1.06279	kg/m^3

Table 4.4 Coefficents for different equivalence ratios of methane

	Methane					
	ER	CH4	Air	CO2	H20	O2
	0.8	1	2.5	1	2	0.5
ER	0.6	1	3.33333	1	2	1.33333
	0.7	1	2.85714	1	2	0.85714
	0.8	1	2.5	1	2	0.5

Table 4.5 Heat of combustion of methane for 0.6, 0.7 and 0.8 equivalence ratios

Methane	Reactants			Prodcuts		
	CH4	O2		CO2	H2O	O2
	1	2.85714		1	2	0.85714
Input temp (K)	298			Qout kJ/kmol	601511.8	
Product temp (K)	1800				37.59	kj/kg
				for 0.6	36.43	kj/kg
				for 0.7	37.59	kj/kg
				for 0.8	38.47	kj/kg

ER	*Tu (K)*	*Tad (K)*	*S_L (m/s)*	*Cp (J/kgK)*	*ρ (kg/m^3)*	*v (m^2/s)*	*δ(Zeldovich) (m)*
1.00	300	2232.27	0.3760	1070.62	1.127	1.61E-05	5.98E-05
0.90	300	2140.94	0.3341	1064.23	1.131	1.60E-05	6.72E-05
0.80	300	2004.19	0.2699	1057.78	1.136	1.60E-05	8.32E-05
0.70	300	1844.65	0.1919	1051.24	1.141	1.60E-05	1.17E-04
0.60	300	1669.95	0.1137	1044.64	1.145	1.60E-05	1.97E-04

Figure 4.13 Equivalence ratio laminar flame speed table from [1]

4.4.1.3 2D Reactive Flow Results:

Premixed combustion of methane is solved in 2D with 0.6, 0.7 and 0.8 equivalence ratios. In figure 4.14 contour plots of progress variables are shown. In 0.6 equivalence ratio the length of the flame is biggest. The laminar flame speed of 0.6 equivalence ratio is 0.1137 m/s

but besides for 0.7 and 0.8 equivalence ratio are 0.1919 and 0.2699 m/s. Increase in laminar flame speed cause decrease in flame length.

In figure 4.15 the comparison of experimental and solution of zimont model on equivalence ratio of 0.6 is shown. The solution of zimont model can be accepted according to figure 4.15. In addition to this in figure 4.16 and figure 4.17 show the comparison of experimental values and zimont model results. In figure 4.16 equivalence ratio is 0.7 besides, in figure 4.17 equivalence ratio is 0.8.

In figure 4.18 the effect of equivalence ratio can be seen. Increase in the equivalence ratio causes decrease in the flame length. The laminar flame speed increases with with increase in the equivalence ratio.

In figure 4.19 shows the velocity that occured in the burner. The velocity streamlines enlarge from tip of the flame.

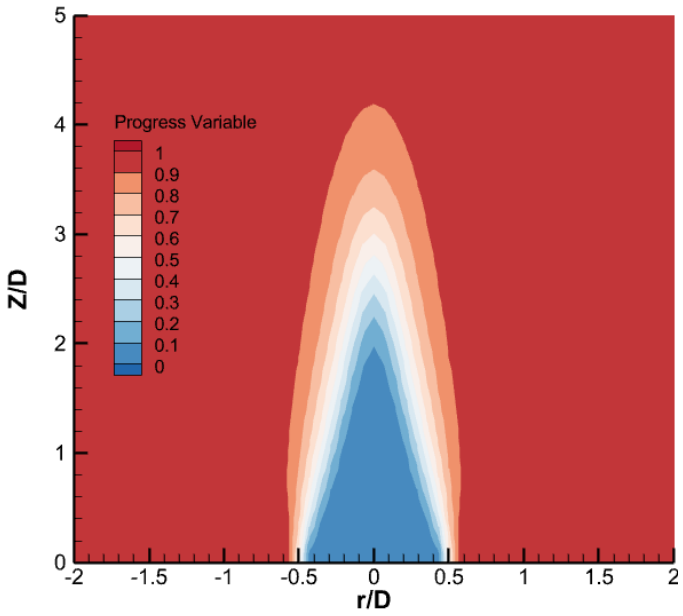

ER= 0.6

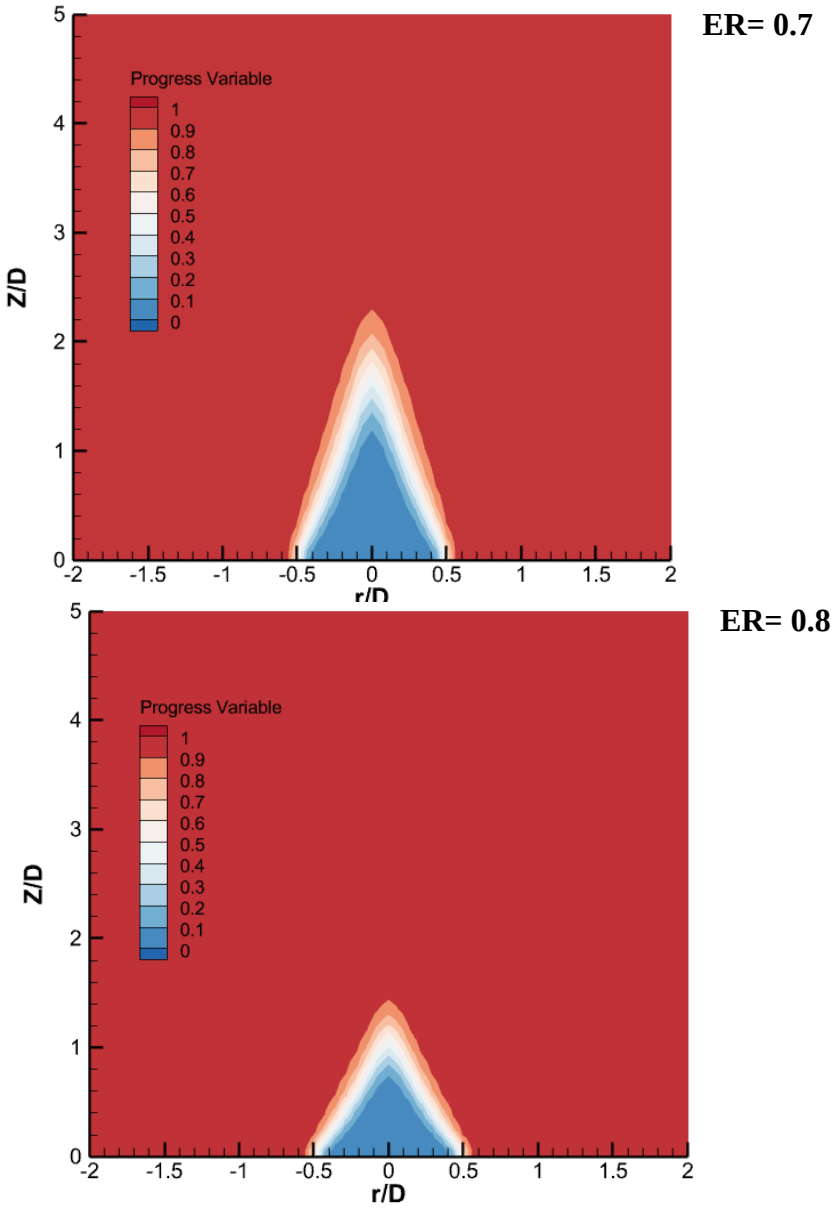

Figure 4.14 The progress variable contour plot of 0.6,0.7 and 0.8 equivalence ratio.

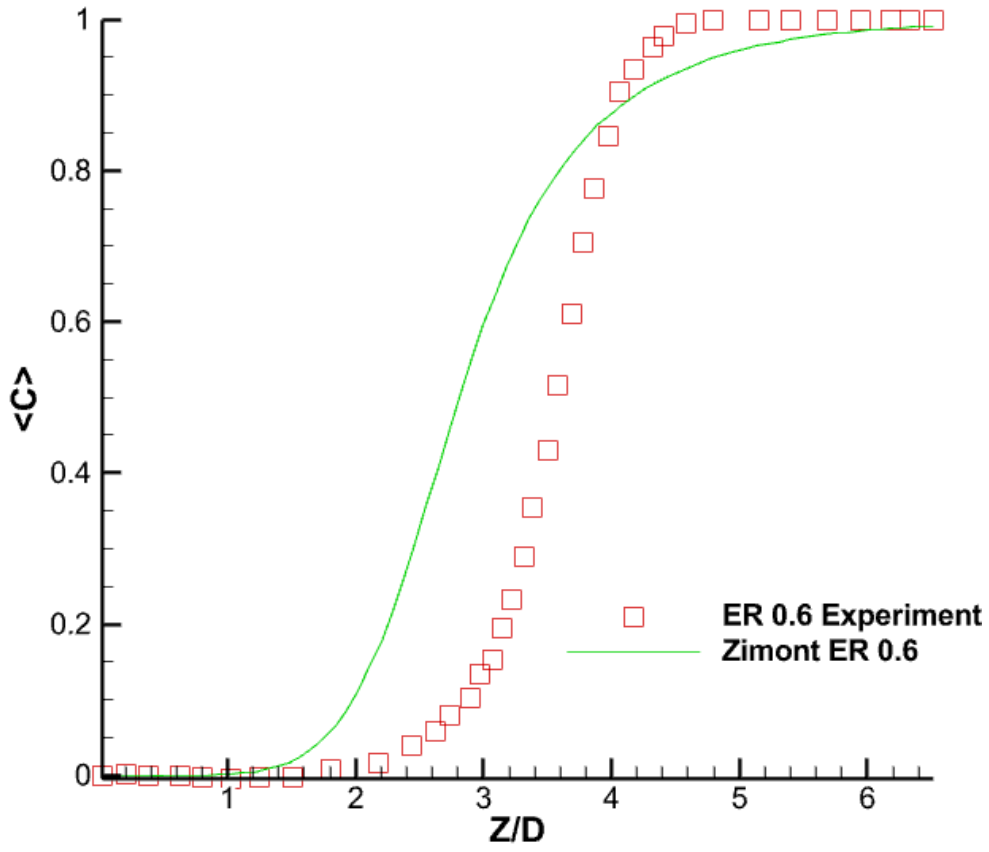

Figure 4.15 The comparison of experimental ER 0.6 and result of Zimont model ER 0.6

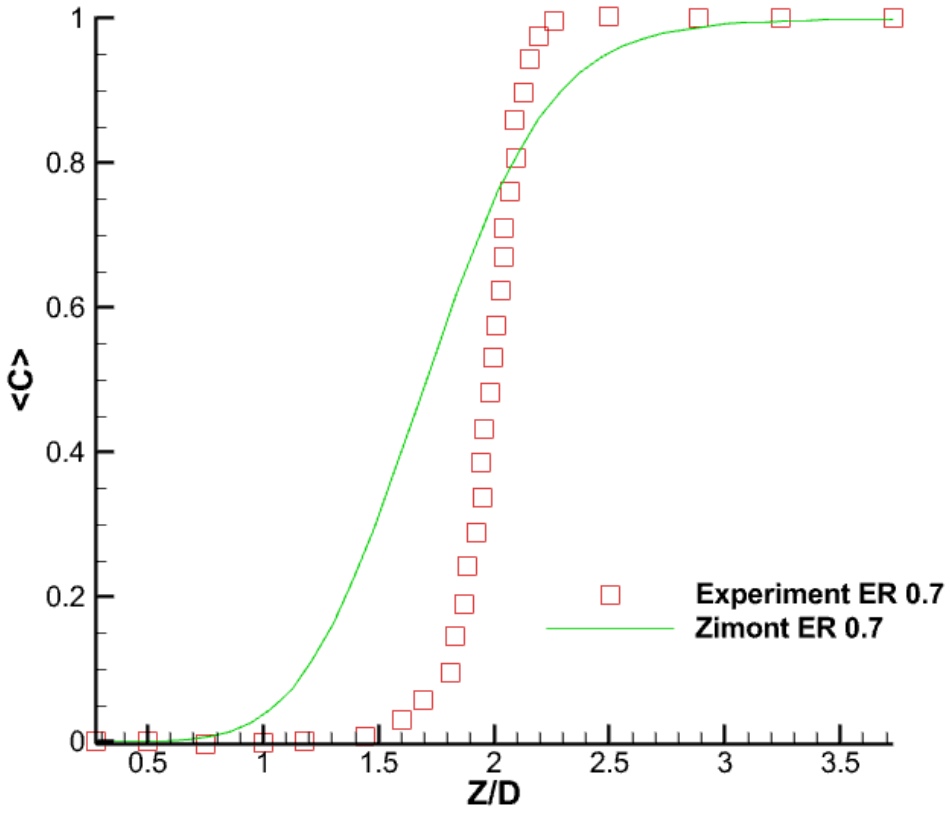

Figure 4.16 The comparison of experimental ER 0.7 and result of Zimont model ER 0.7

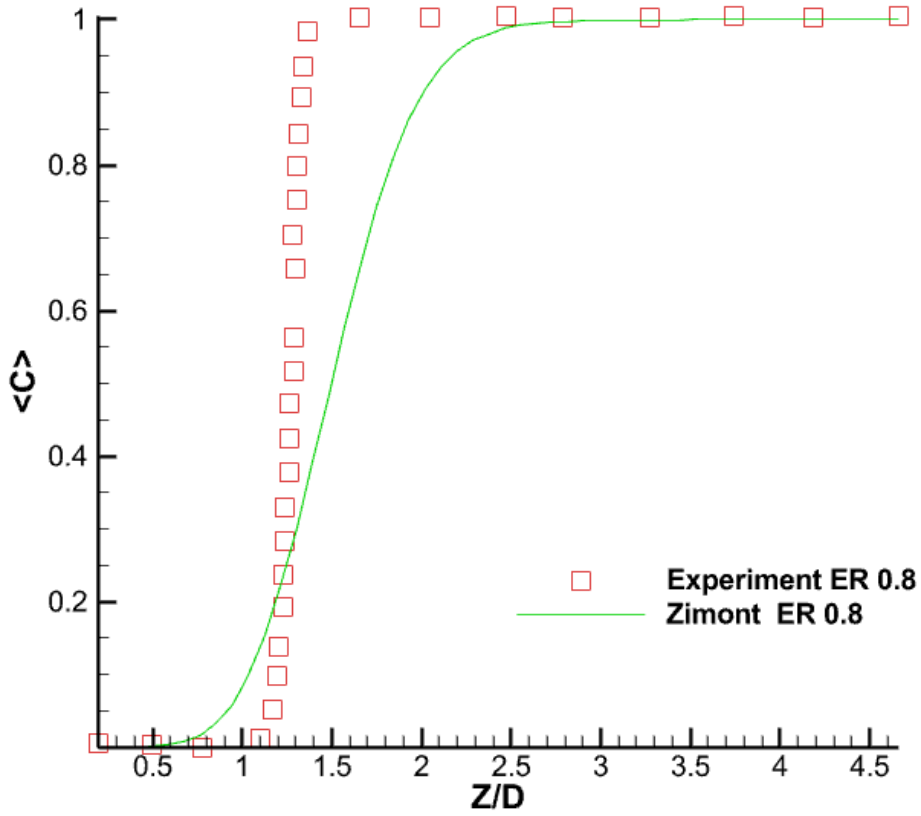

Figure 4.17 The comparison of experimental ER 0.8 and result of Zimont model ER 0.8

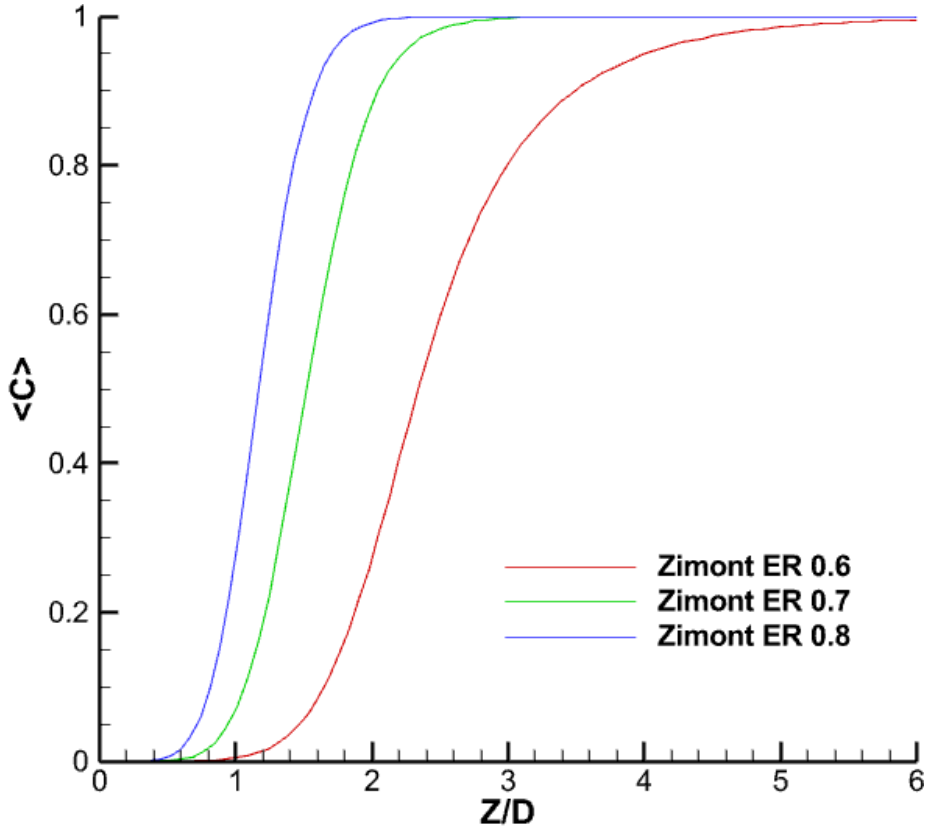

Figure 4.18 The comparison result of Zimont model ER 0.6,0.7,0.8

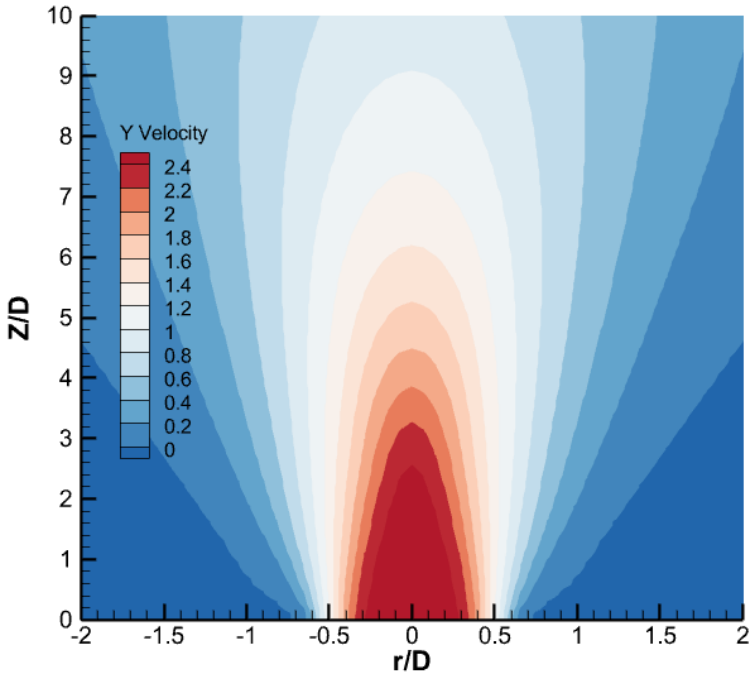

Figure 4.19 Axial velocity that occured on ER 0.6

In figure 4.20 the velocity streamline and progress variable lines are shown. The velocities enlarge from the sides of the flame. But in progress variable there is no change in bell curved shape of flame from starting point to finishing point. In figure 4.21 turbulent kinetic energy and progress variable can be seen in one figure.

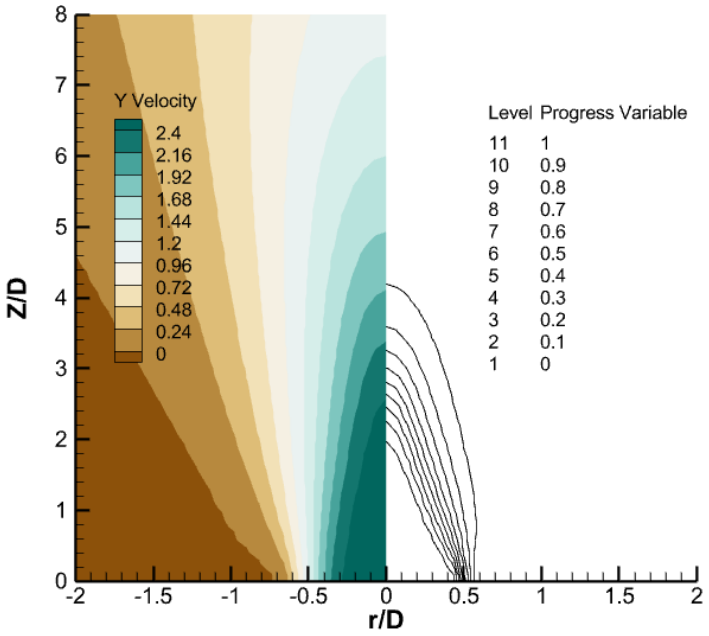

Figure 4.20 Axial velocity and progress variable on ER 0.6

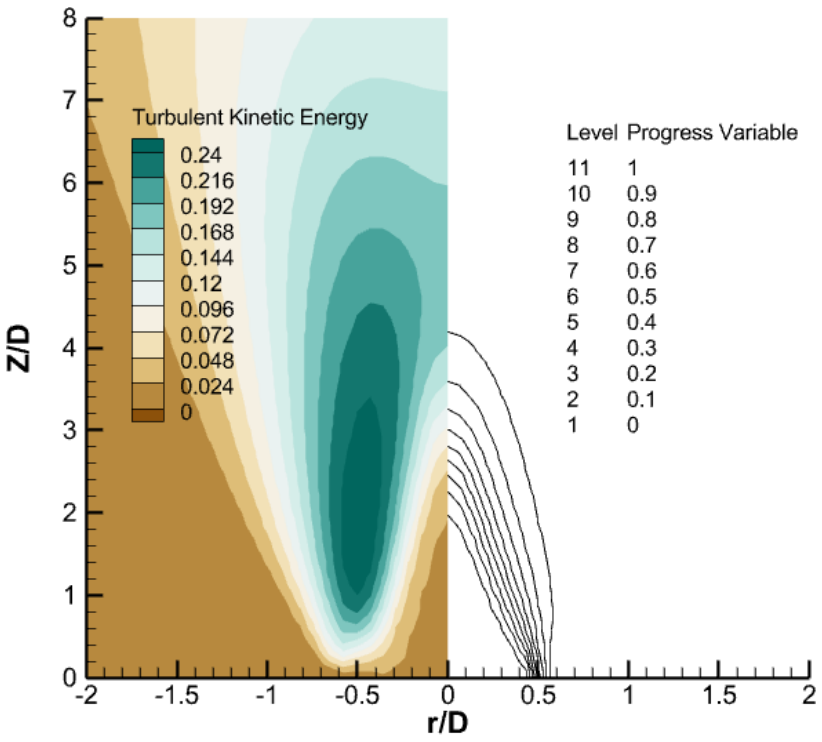

Figure 4.21 Turbulent kinetic energy and progress variable on ER 0.6

4.4.2 3D Cold Flow

After deciding on the mass flow rate, the velocity profile is obtained as seen in figure 4.22

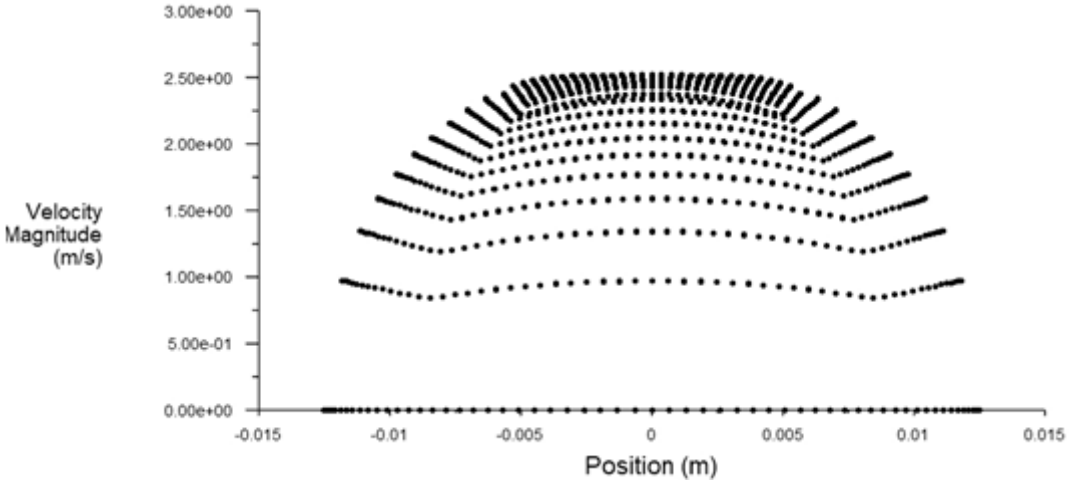

Figure 4.22 Fully developed velocity profile

The velocity profile is exported as a data file and later it is inserted input boundary condition when the burner is analyzed.

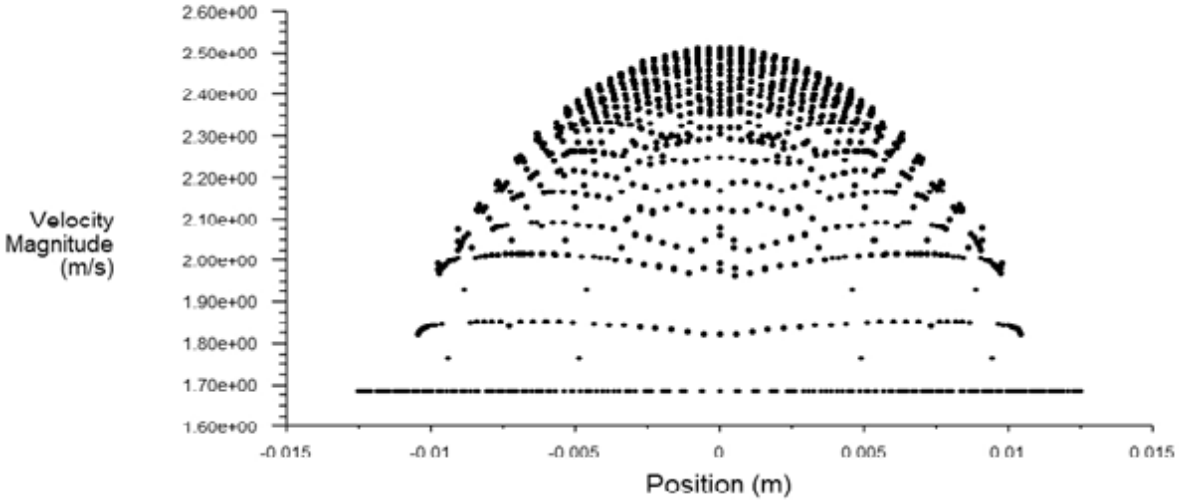

Figure 4.23 Velocity Profile with coarse Mesh

As seen in figure 4.23, the velocity profile is obtained with coarse mesh, and it is used in the beginning, but it affects wrong the whole result.

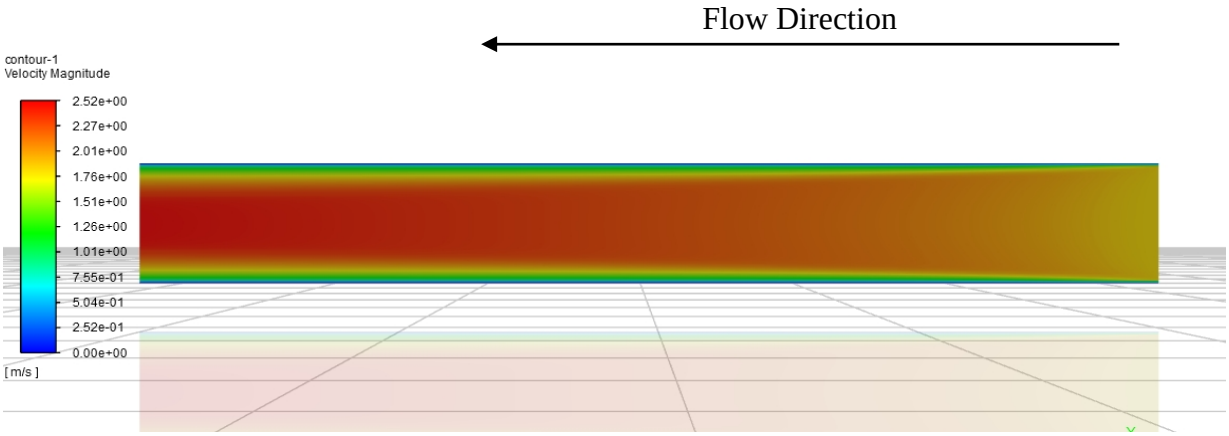

Figure 4.24 Cold flow velocity contour

4.4.2.3 Cold Flow Analysis in Combustion Chamber:

Finally, outlet axial velocity is inserted as velocity inlet. It is used for 3-D analysis.

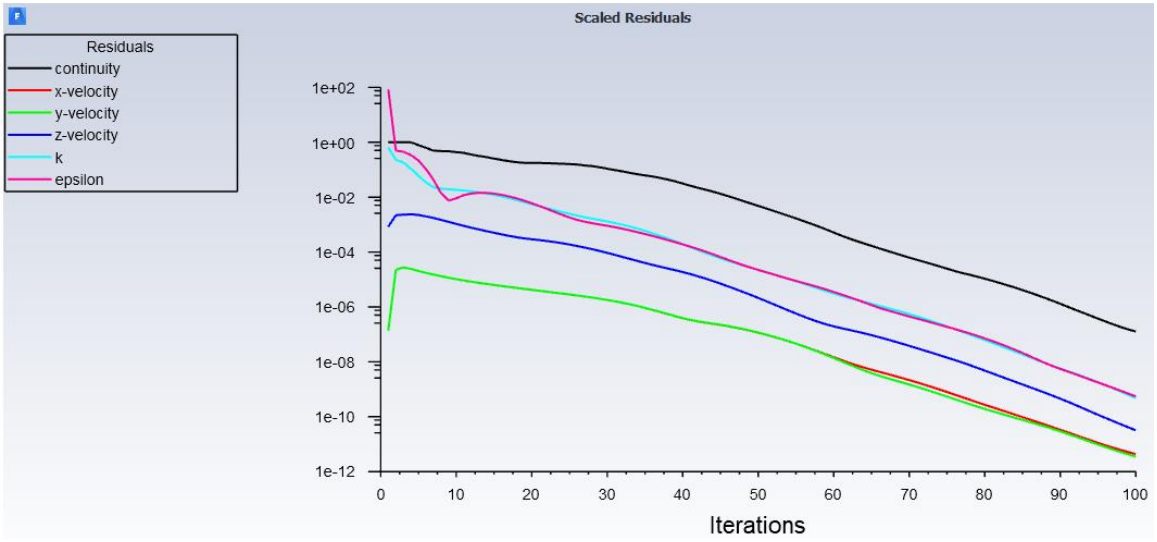

Figure 4.25 Continuity values with iteration

Table 4.6 k-epsilon model vs iteration

K-epsilon model	Iteration
Standard	63
RGN	77
Realizable	111

After the solution, the realizable model is chosen as the k-epsilon model according to figure 4.26 and the Halter value and realizable value almost fit each other. So, k-epsilon realizable model is selected for the combustion model in the next stage.

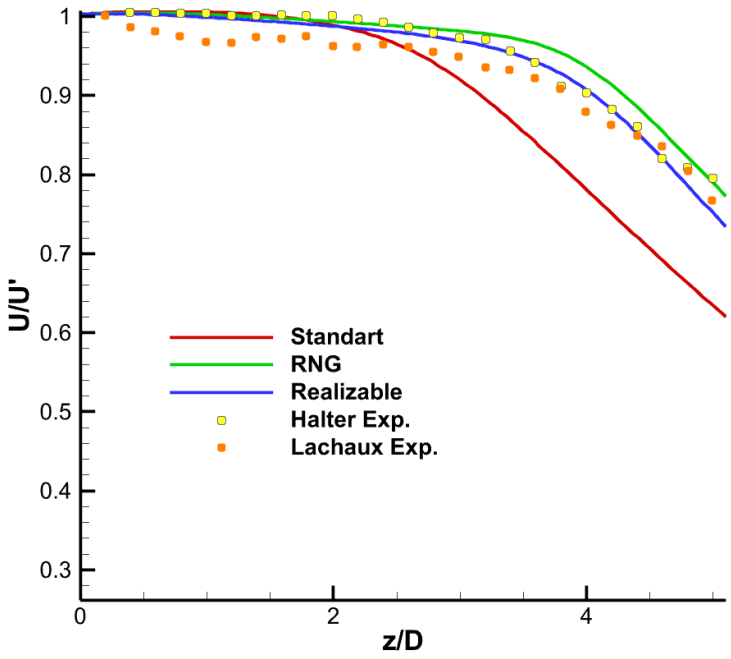

Figure 4.26 The predicted axial velocity profiles with different k-e model variants versus the normalized axis

4.4.2.5 Combustion Chamber Mesh Indepence:

As shown in figure 4.27 mesh independence analysis is made with respect to the 0.6 ER Halter value. When the node is increased, the value is getting closer to Halter's experiment values. Nodes could have increased more but computer performance is not enough to perform meshing processes.

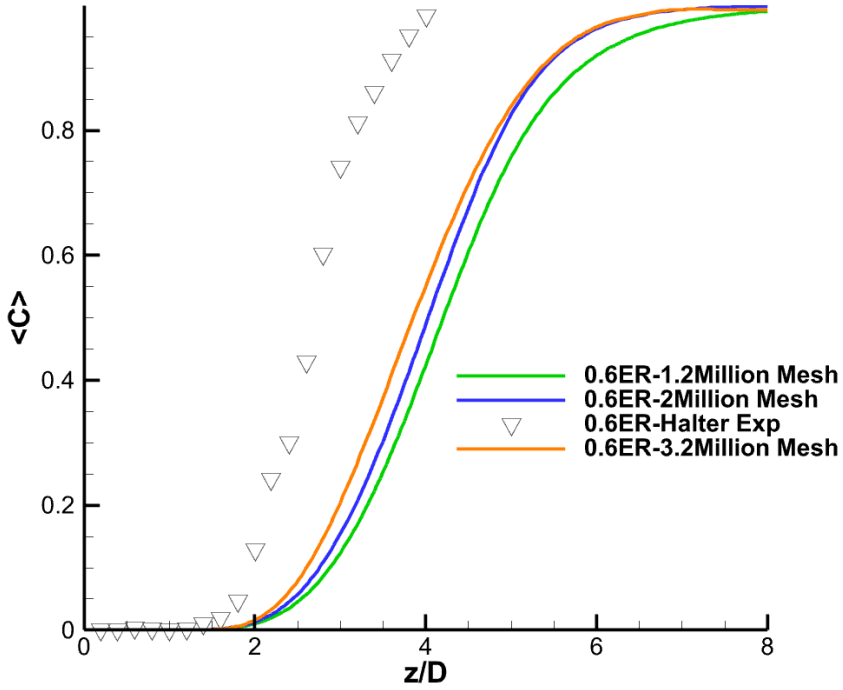

Figure 4.27 Mesh Independence Analysis

4.4.2.6 3-D Combustion Chamber

3-D analysis setup is the same boundary condition, model, method etc. as 2-D. So, the same process is applied. After inserting setup processing, the solutions are converged at different iterations because of the equivalent ratio.

The continuity reaches 10^{-6} values. It is acceptable for post-processing. In addition, it occurs fluctuations in the residuals graph because momentum, turbulent kinetic energy, and turbulent dissipation rate is solved in the first order at the beginning after that these are changed in the second order. The converged values are reached sooner, and the computer is used more efficiently with helping this process.

Table 4.7 Iteration number vs ER

	Iteration
ER=0.6	3800
ER=0.7	3560
ER=0.8	3985

4.4.2.7 3-D Post Processing:

Figure 4.28 shows that the more CH_4 (methane) is added, the shorter the flame length. In addition, when laminar flame speed is getting higher, the flashback effect is getting more. That is why flame length is shorter at a small equivalent ratio. Respectively, the laminar flame speed is 0.1136 m/s, 0.1919 m/s, 0.2699 m/s at 0.6 ER, 0.7 ER, and 0. 8 ER.Thus, the flashback effect is more at 0.8 compared to 0.6 ER. As a result of this, flame length is shorter at 0.8 ER.

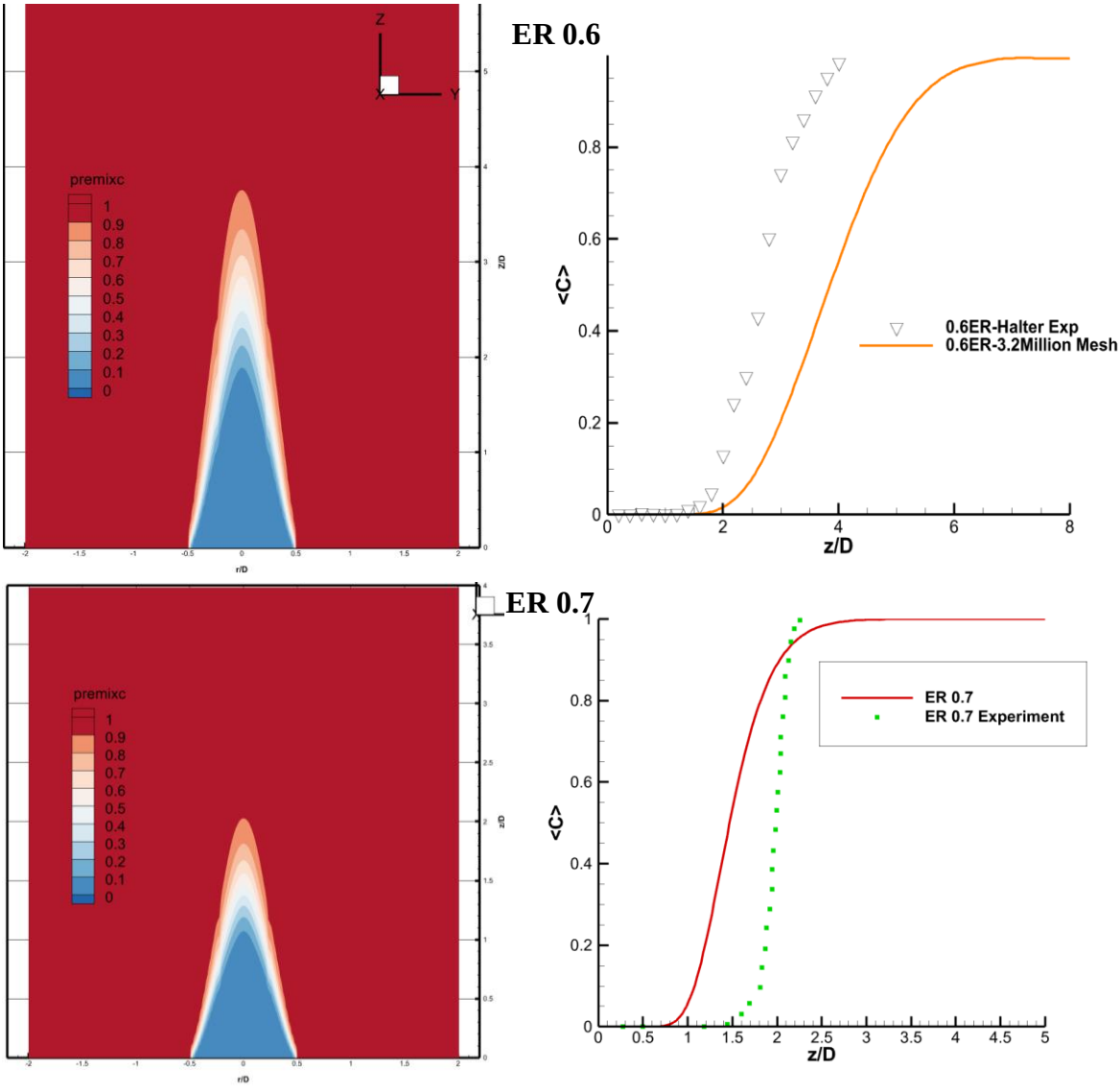

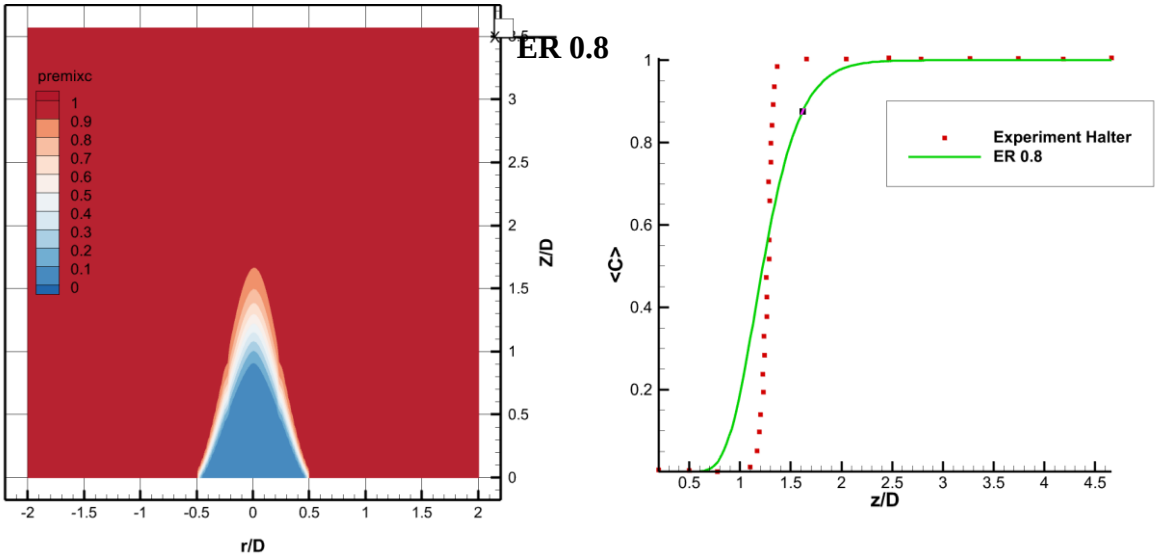

Figure 4.28 Contour and XY plots of progress variable at 0.6 ,0.7 and 0.8 ER

4.4.3 Hydrogenated Methane:

4.4.3.1 Hydrogenated Methane Setup:

After when the methane combustion with different equivalence ratios of 0.6, 0.7, 0.8 has done the material had been changed with properties of %10 and %20 H_2. Firstly, the equation of combustion of hydrogenated methane is solved with 0.6 equivalence ratio. Methane ratio is set %10 and %20 of volume percentage. The heat of combustion and density is calculated by Excel software.

		Methane+Hydrogen							
		ER	CH4	H2	Air		CO2	H20	O2
		0.6	0.8	0.2	2.768334768		0.8	1.8	1.06833
ER=0.6	H2	5%	0.95	0.05	3.20833		0.95	1.95	1.2833
		10%	0.9	0.1	3.061667		0.9	1.9	1.21167
		20%	0.8	0.2	2.768335		0.8	1.8	1.06833

Methane+H2	Reactants				Prodcuts		
	CH4	O2	H2		CO2	H2O	O2
	0.8	3.20833	0.2		0.8	1.8	1.50833
Input temp (K)	298				Qout kJ/kmol	530653.6702	
Product temp (K)	1800					33.17	kj/kg
					0.6 %5 H2	35.84	kj/kg
					0.6 %10 H2	34.95	kj/kg
					0.6 %20 H2	33.17	kj/kg

Figure 4.29 Coefficient and heat of combustion table

In figure 4.29 the coefficient of methane-hydrogen mixture and heat of combustion values can be seen. The related heat of combustion and laminar flame speed that is in Figure 4.30 are written in material menu for hydrogenated methane solution. Then, the solution procedure that is explanied in the previous sections is applied to solve the methane-hydrogen mixture flame.

ER	*Tu (K)*	*Tad (K)*	*S_L (m/s)*	*Cp (J/kgK)*	*ρ (kg/m^3)*	*ν (m^2/s)*	*δ(Zeldovich) (m)*
1.00	300	2232.27	0.3760	1070.62	1.127	1.61E-05	5.98E-05
0.90	300	2140.94	0.3341	1064.23	1.131	1.60E-05	6.72E-05
0.80	300	2004.19	0.2699	1057.78	1.136	1.60E-05	8.32E-05
0.70	300	1844.65	0.1919	1051.24	1.141	1.60E-05	1.17E-04
0.60	300	1669.95	0.1137	1044.64	1.145	1.60E-05	1.97E-04

Figure 4.30 Phsysical properties of methane-hydrogen mixture that is get from [1]

4.4.3.2 3D Results:

The contour plots that are in figure 4.31 shows the progress variable of the hydrogenated-methane flame. In %0 H_2 condition the flame is bigger than %10 H_2 and %20 H_2 condition. The reason caused by the laminar flame speed increases of higher hydrogen percentages. Besides, the hydrogen has lower heat of combustion than methane. Therefore, both hydrogen have less heat of combustion value and hydrogen has higher laminar flame speed and higher flashback occurance. When the hydrogen percentage of the mixture is increased the flame length is decreased.

In figure 4.32 the progress variable of different percentages of hydrogentaed methane graph can be seen. In that graph the increase in the hydrogen percentage causes decrease in the flame length.

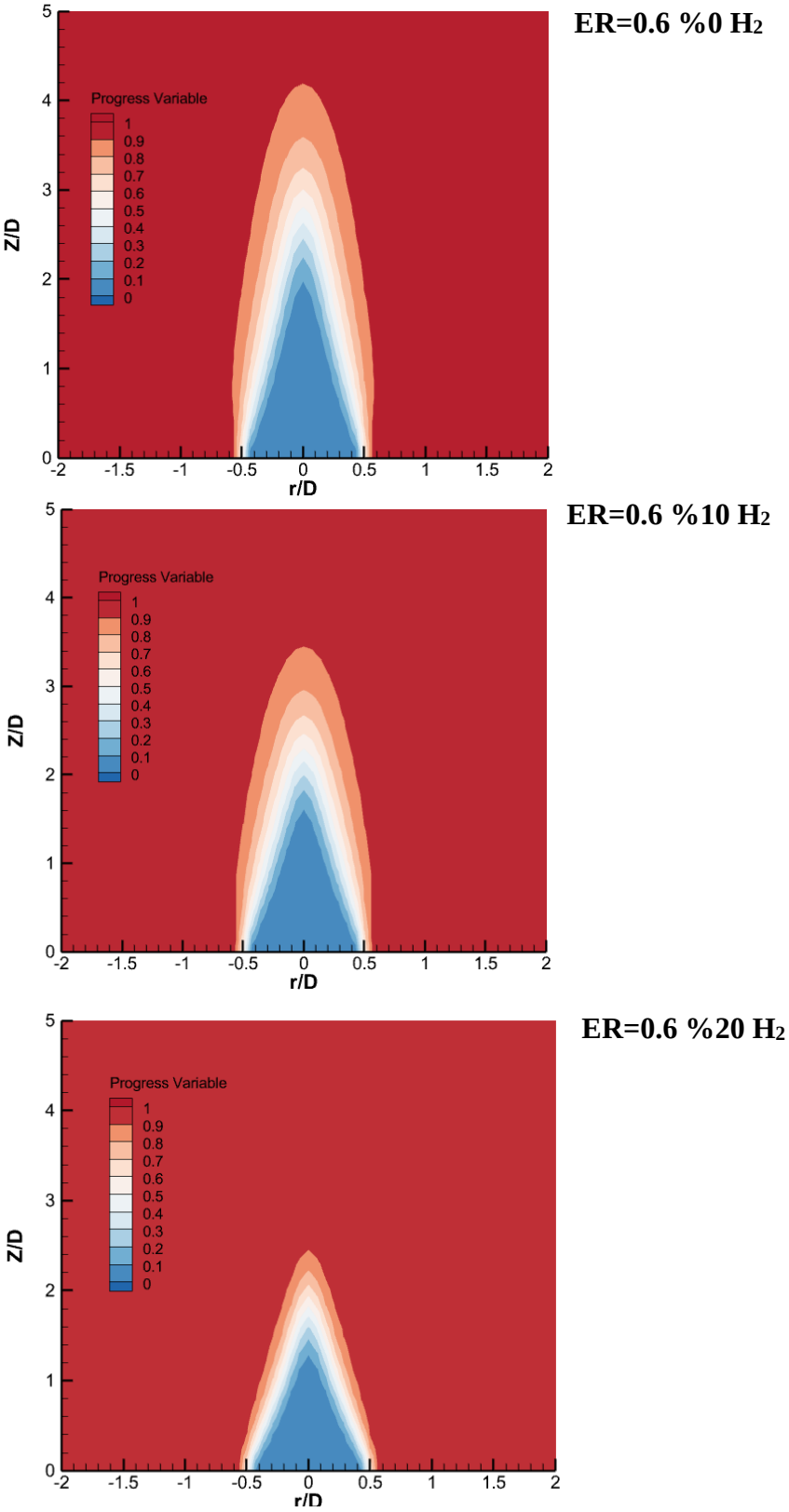

Figure 4.31 Hydrogenated-methane progress variable contour plots

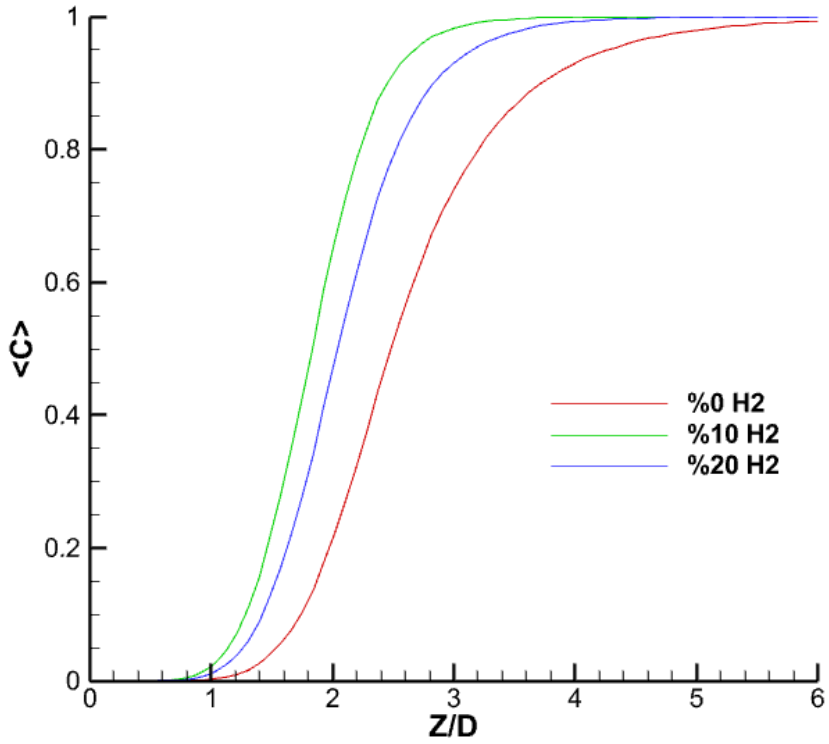

Figure 4.32 Progress variables graph of hydrogenated methane

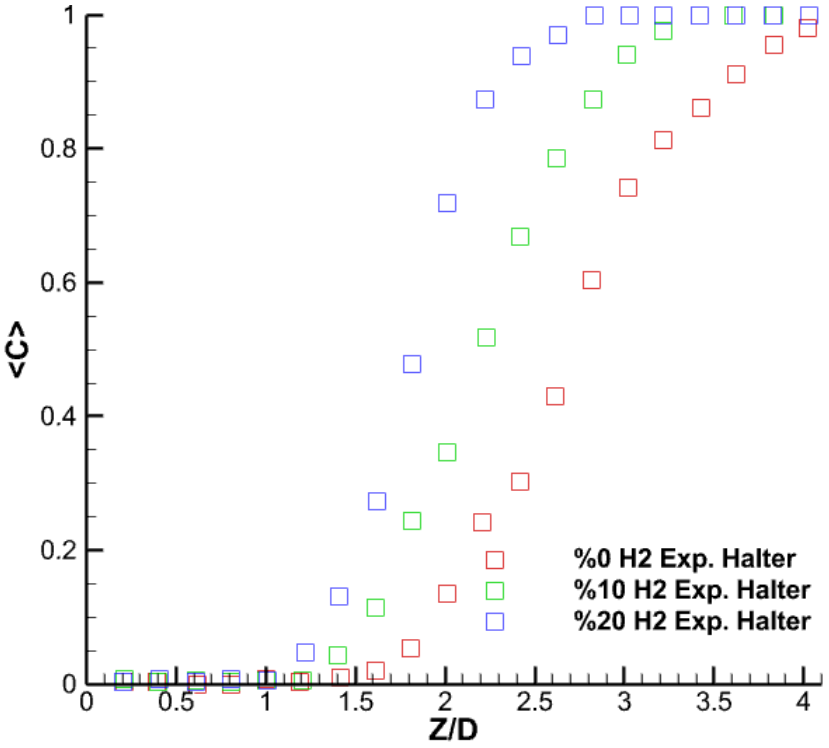

Figure 4.33 Experimental results of Halter progress variables graphs of hydrogenated-methane

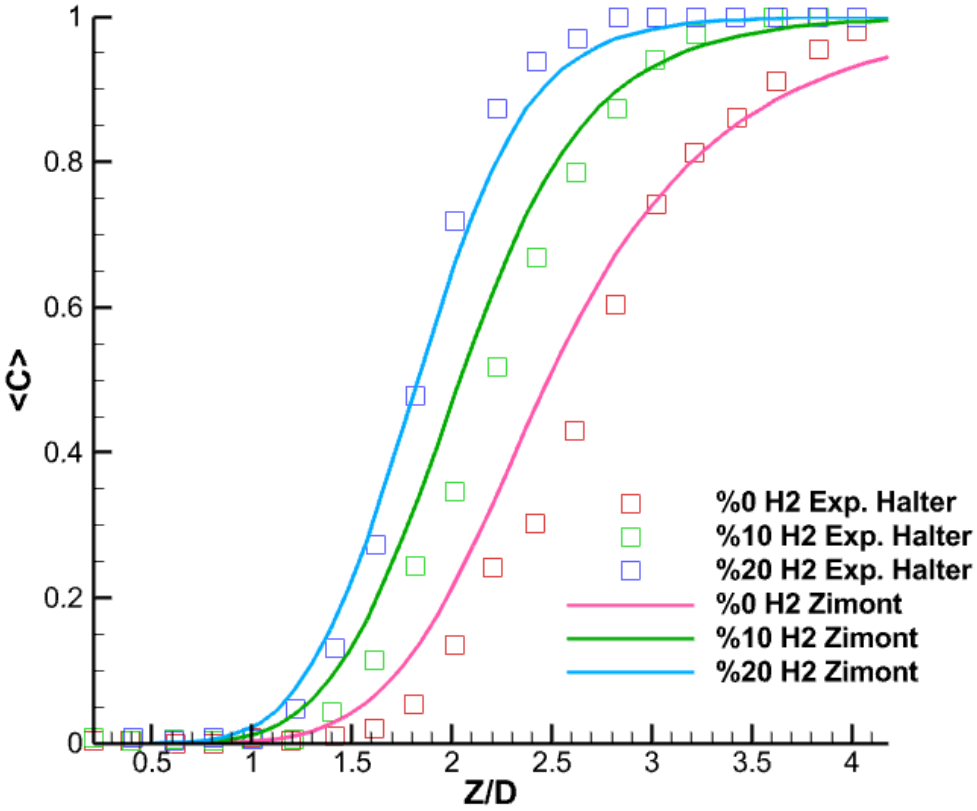

Figure 4.34 Experimental results and Zimont model results comparison

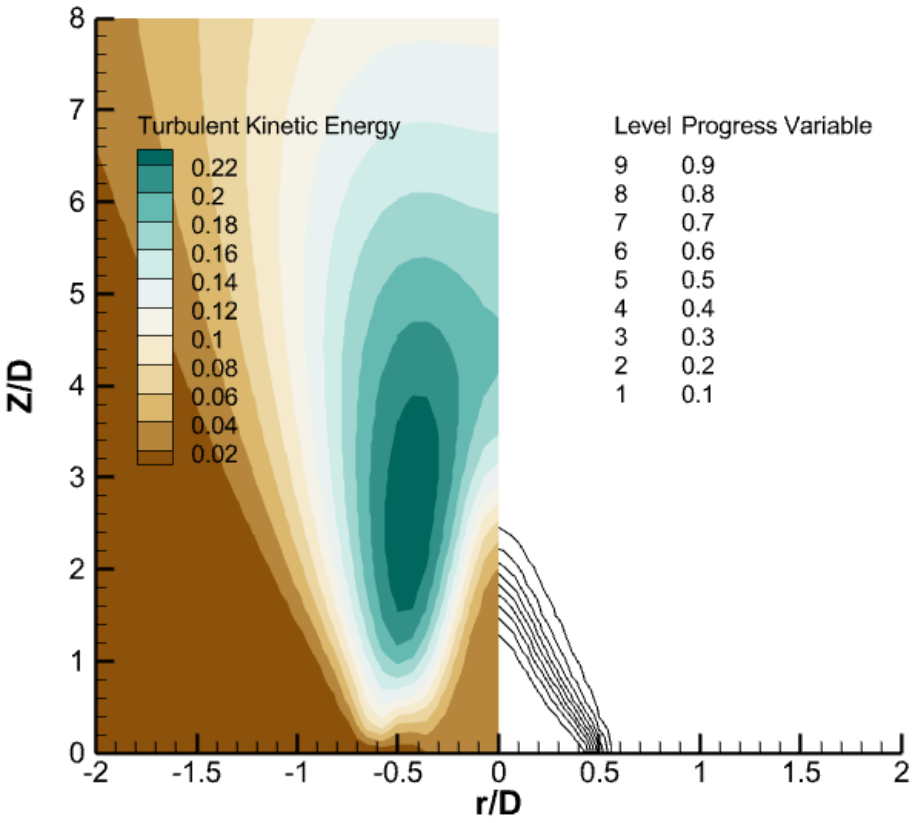

Figure 4.35 Turbulent kinetic energy and progress variable graph on %20 H2 combustion

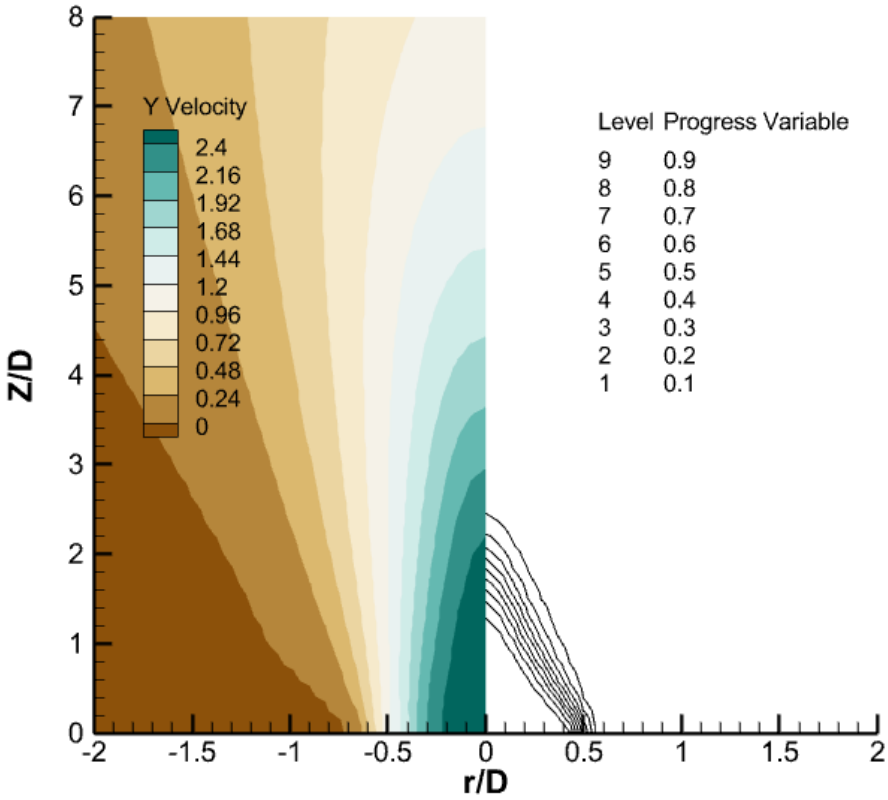

Figure 4.36 Velocity and progress variable graph on %20 H2 combustion

5.CONCLUSIONS

The methane and hydrogenated-methane combustion have been numerically computed in the present study. The simulation results of methane and hydrogenated-methane combustion is validated the results that are taken from experiment of Halter and Lachaux. The modeling study have been started to analyze cold flow. Then, the grid independent solution and method selection have been solved and the method that is used selected. After that, the methane and hydrogenated-methane flame simulations have been performed. The effects of equivalence ratio change have been observed and compared with experimental results of Halter and Lachaux.

At the beginning the simulation 2D reactive and cold flow have been performed firstly. Then, the results of this simulations have been compared with the experimental results of Halter and Lachaux. The best results of cold flow have been got from the Realizable model and 1 mm mesh sizing. The Realizable model and 1 mm mesh sizing have been used in 2D and 3D reactive flows.

In 3D flow simulations the meshing type and sizing have been found by making developments on the meshing. Firstly, in meshing process, the meshing has been tried to make structured. After that, the mesh element quality has been tried to make acceptable element quality values of 0.3. The 3D meshing quality has been made acceptable. Then, the 3D cold and reactive flow simulations have been solved by Ansys Fluent.

For equivalence ratio of 0.6, 0.7 and 0.8 methane combustion equation have been solved via a basic Excel page. The coefficients of combustion products and reactants have been found. Besides, the heat of combustion and density values of methane for 0.6, 0.7 and 0.8 equivalence ratios have been solved by an Excel page. In 3D simulation of reactive flow, the equivalence ratio of 0.6 have been solved firstly. Then 0.7 and 0.8 equivalence ratio methane combustion simulations have been performed.

After that, the heat of combustions and densities of hydrogenated-methane have been found on an Excel page. Then the material properties of hydrogen-methane mixture are used for flame simulation. Then, hydrogenated-methane for %10 and %20 volumetric percentage of hydrogen simulations have been performed.

Then, the results of reactive flow of 2D and 3D simulations have been compared with different equivalence ratios and experimental data of Halter and Lachaux. The equivalence ratio effects the flame length. For methane flame simulations increase in equivalence ratio causes

increase in flame length of methane. Besides, in hydrogenated-methane flame the increase in volumetric hydrogen percentage of mixture cause decrease in flame length. Besides, increase in volumetric hydrogen percentage causes decrease in laminar flame speed. Higher laminar flame speed forms a risk for flashback effect.

REFERENCES:

[1] YILMAZ, Barıs., Computational Analysis And Experimental Verification Of Premixed Combustion Of Hydrogen Methane/Air Mixtures, PhD Thesis, Istanbul, 2010.

[2] Gökalp, Iskender; "Clean Combustors for Industrial Gas Turbines", Von Karman Institute for Fluid Dynamics Lecture Series Notes 2003-2004. Edited by R. Denos, Rhode Saint Genese, Belgium (2004).

[3] Yu, G.; Law, C. K.; Wu, C. K.: "Laminar Flame Speeds of Hydrocarbon + Air Mixtures with Hydrogen Addition", Combust and Flame 63 (1986) 339–347.

[4] Paris Agreement, article 2, pg. 5

[5] Han W, Dai P, Gou X, Chen Z. A review of laminar flame speeds of hydrogen and syngas measured from propagating spherical flames. Applications in Energy and Combustion Science 2020;1:100008.

[6] Shu J, Fu J, Liu J, Wang S, Yin Y, Deng B, et al. Influences of excess air coefficient on combustion and emission performance of diesel pilot ignition natural gas engine by coupling computational fluid dynamics with reduced chemical kinetic model. Energy Convers Manag 2019;187:283e96.

[7] Wang J, Li Y, Xia H, Ju R, Zhang M, Mu H, et al. Effect of hydrogen enrichment and electric field on lean CH_4/air flame propagation at elevated pressure. Int J Hydrogen Energy 2019;44:15962e72.

[8] Pan J, Zheng Z, Wei H, Pan M, Liang X. An experimental investigation on pre-ignition phenomena: emphasis on the role of turbulence. Proc Combust Inst 2020;38(4):5801e10.

[9] Zhang Y, Gerdroodbary MB, Hosseini S, Abazari A, Li Z. Effect of hybrid coaxial air and hydrogen jets on fuel mixing at supersonic crossflow. Int J Hydrogen Energy 2021;46:16048e62.

[10] Jiang Y, Poozesh A, Marashi SM, Moradi R, Gerdroodbary MB, Shafee A, et al. Effect of cavity back height on mixing efficiency of hydrogen multi-jets at supersonic combustion chamber. Int J Hydrogen Energy 2020;45:27828e36.

[11] Sun ZY. Structure of turbulent rich hydrogen-air premixed flames. Int J Energy Res 2018;42:2845e58.

[12] Gerdroodbary MB, Mokhtari M, Fallah K, Pourmirzaagha H. The influence of micro air jets on mixing augmentation of transverse hydrogen jet in supersonic flow. Int J Hydrogen Energy 2016;41:22497e508.

[13] Bhasker JP, Porpatham E. Effects of compression ratio and hydrogen addition on lean combustion characteristics and emission formation in a Compressed Natural Gas fuelled spark ignition engine. Fuel 2017;208:260e70.

[14] Bhasker JP, Porpatham E. Effects of compression ratio and hydrogen addition on lean combustion characteristics and emission formation in a Compressed Natural Gas fuelled spark ignition engine. Fuel 2017;208:260e70.

[15] Sun ZY. Structure of turbulent rich hydrogen-air premixed flames. Int J Energy Res 2018;42:2845e58.

[16] Hu E, Huang Z, He J, Jin C, Zheng J. Experimental and numerical study on laminar burning characteristics of premixed methaneehydrogeneair flames. Int J Hydrogen Energy 2009;34:4876e88.

[17] Gerdroodbary MB, Mokhtari M, Fallah K, Pourmirzaagha H. The influence of micro air jets on mixing augmentation of transverse hydrogen jet in supersonic flow. Int J Hydrogen Energy 2016;41:22497e508.

[18] Wang J, Huang Z, Tang C, Zheng J. Effect of hydrogen addition on early flame growth of lean burn natural gaseair mixtures. Int J Hydrogen Energy 2010;35:7246e52.

[19] Stephen R. Turns, An Introduction To Combustion Concepts And Applications Third Edition

[20] Numerical And Experimental Investigation Of A Domestic Natural Gas Burner And Analysis Of Modifications To Achieve Low Nox Emissions Engin Uza Master Thesis

[21] ANSYS FLUENT 12.0 Theory Guide - 9.3 Extended Coherent Flamelet Model Theory (enea.it)

[22] Zimont, V.; Polifke, W.; Bettelini, M.; Weisenstein, W.: "An efficientcomputational model for premixed turbulent combustion at high Reynolds numbers based on a turbulent flame speed closure", J. of Gas Turbines Power, 120 (1998) 526-532.

[23] Zimont, V.L.: "Gas premixed combustion at high turbulence. Turbulent flame closure combustion model", Exp. Thermal and Fluid Science, 21 (2000) 179-186.

[24] Borghi R.: "On the Structure and Morphology of Turbulent Premixed Flames", Rec. Adv. Aerosp. Sci. (1985) 117-138

[25] Lachaux, T.: "Etude des effets de la haute pression sur la structure et la dynamique des flammes turbulentes de prémélange pauvre de méthane-air", PhD Thesis, Universite d'Orleans, Orleans, France, (2004).

[26] Halter, F.: "Caracterisation des effets de l'ajout d'ajout d'hydrogene et de la haute pression dans les flammes turbulentes de premelange Methane/Air",

[27] ANSYS FLUENT 12.0 Theory Guide - 9.2.1 Propagation of the Flame Front (enea.it)

[28] Cengel, Y: Thermodynamics: An Engineering Approach, 8th edition